Experimental study of high to intermediate temperature alteration in porphyry copper systems and geological implications

Article *in* Science China Earth Science · December 2018

DOI: 10.1007/s11430-018-9295-1

CITATIONS
0

READS
265

5 authors, including:

Li Jianping
Chinese Academy of Sciences
1 PUBLICATION **0** CITATIONS
SEE PROFILE

Huayong Chen
Chinese Academy of Sciences
96 PUBLICATIONS **1,545** CITATIONS
SEE PROFILE

Bing Xiao
Guangzhou Institute of Geochemistry, Chinese Academy of Sciences, Guangzhou
30 PUBLICATIONS **223** CITATIONS
SEE PROFILE

SCIENCE CHINA
Earth Sciences

•RESEARCH PAPER•

March 2019 Vol.62 No.3: 550–570
https://doi.org/10.1007/s11430-018-9295-1

Experimental study of high to intermediate temperature alteration in porphyry copper systems and geological implications

Jianping LI[1,2], Huayong CHEN[1*], Long SU[3†], Bing XIAO[1] & Yunfeng WANG[1,2]

[1] *Key Laboratory of Mineralogy and Metallogeny/Guangdong Provincial Key Laboratory of Mineral Physics and Materials, Guangzhou Institute of Geochemistry, Chinese Academy of Sciences, Guangzhou 510640, China;*
[2] *University of Chinese Academy of Sciences, Beijing 100049, China;*
[3] *Key Laboratory of Petroleum Resources, Gansu Province/Key Laboratory of Petroleum Resources Research, Institute of Geology and Geophysics, Chinese Academy of Sciences, Lanzhou 730000, China*

Received April 17, 2018; revised October 8, 2018; accepted October 30, 2018; published online December 28, 2018

Abstract Porphyry copper systems, which provide most of the world's copper resource, are commonly associated with characteristic concentric zonation of alteration and mineralization. In-depth knowledge of the distribution and transport mechanism of elements in the alteration zones is essential for understanding the ore-forming processes. We employed flow-reaction apparatus to simulate the fluid-rock interactions during porphyry ore formation so as to investigate the mechanisms that govern the transport of elements and the development of zonation. The results indicate more heterogeneous distribution of elements in the experimental products at 450°C compared to those at lower temperatures, which implies a crucial role of temperature in controlling elements redistribution in hydrothermal systems. Heating advances potassic alteration and Ca leaching of wall rocks. To achieve the same degree of sodic alteration, it requires a higher concentration of Na^+ in the fluid toward higher temperature. Temperature also facilitates the incorporation of Ti, Sr and Pb into silicate minerals through cation substitution. We infer from experimental results that from the center of intermediate to mafic volcanic wall rocks toward periphery, the contents of K and Ti should decrease and the contents of Ca, Zn and Mn should increase, whereas the trend for Si and Na could be non-monotonic. This study provides experimental and theoretical insights into a variety of vital geological observations, including anhydrite formation and the widespread development of potassic rather than sodic alteration in porphyry copper deposits.

Keywords Porphyry copper deposit, Fluid-rock interactions, Flowing systems, Elements transport mechanism

Citation: Li J, Chen H, Su L, Xiao B, Wang Y. 2019. Experimental study of high to intermediate temperature alteration in porphyry copper systems and geological implications. Science China Earth Sciences, 62: 550–570, https://doi.org/10.1007/s11430-018-9295-1

1. Introduction

Porphyry copper (Cu) deposits have supplied nearly three-quarters of the world's Cu, half the Mo, around one-fifth of the Au, and significant amounts of other precious/base metals, such as Ag, Zn, and Pb (Sillitoe, 2010; Cooke et al., 2014b). Most porphyry-related mineralization occurs in subduction zones, and is closely associated with oxidized adakitic magma. Tectonically, the mineralization occurs in compressive settings, notably around the Pacific Rim (Sillitoe, 1972; Kerrich, 2000; Cooke et al., 2005, 2014b; Chen and Xiao, 2014). At the convergent plate boundaries, the melting of the subducted oceanic slab and/or the overlying mantle wedge is triggered by slab dehydration, and the hydrous oxidized magma is formed subsequently (Ringwood, 1977; Richards and Kerrich, 2007; Richards, 2011; Sun et al., 2010). Interactions between the melt and the lower continental crust (MASH process) produce more silica-rich magma and form shallow magma chambers, where magma

* Corresponding author (email: huayongchen@gig.ac.cn)
† Corresponding author (email: longsu@lzb.ac.cn)

migrates upward through fault systems and exsolves metal-rich hydrothermal fluid by decompression (Hildreth and Moorbath, 1988; Harris et al., 1990; Landtwing et al., 2005). Deposition of metals in confined space (apex of the porphyritic intrusions) ultimately causes porphyry-type mineralization. During the fluid flow, the exsolved ore-forming fluids alter the surrounding intrusions and country rocks, and a variety of mineralization and alteration zones are developed. Porphyry Cu deposits usually display a successive concentric zonation of alteration and mineralization, featured by potassic alteration in the center and surrounded by the almost-coeval propylitic alteration. Sericite, argillic and advanced-argillic alterations are commonly formed later and superimpose on the earlier alteration zones (Lowell and Guilbert, 1970; Sillitoe, 2010). The early-formed, high-temperature potassic alteration zone is mainly distributed in the apex of the causative intrusion and the immediate surrounding country rocks. The transition from magma into magmatic fluid is also crucial for extracting metals and sulfur from the melt into the fluid. For most porphyry deposits, the potassic alteration zone hosts the bulk of the orebodies, and contains a common mineral assemblage of K-feldspar, biotite, quartz, anhydrite, magnetite and Cu-Fe sulfides (Sillitoe, 1973; Cooke et al., 2014b). Therefore, investigations on alteration zoning in porphyry Cu systems, especially on the formation mechanism, controlling factors and elemental behavior in the high- to intermediate-temperature alteration zones, can reveal the ore-forming fluid evolution and mineralization process. Conventional research techniques for hydrothermal ore deposits mainly rely on geological and microscopic petrographic observations and fluid inclusion measurement, in combination with alteration mineral assemblages and stable isotope compositions to identify the physicochemical alteration/mineralization conditions, e.g., fluid source, temperature, fO_2, pH, salinity and major fluid compositions. The reliability of these conventional techniques, however, is hampered by the complex syn-/post-mineralization modifications, such as the multistage magmatic-hydrothermal overprinting that forms secondary fluid inclusions and alteration mineral assemblages.

With the development of advanced experimental methods and analytical techniques, selecting suitable geochemical models to experimentally investigate geological process has become increasingly effective. Chemical equilibrium theory provides the foundation to understand fluid-rock interactions in closed system, and it can also be used to solve some equilibrium thermodynamic and kinetic issues (Helgeson, 1969; Ré et al., 2014). Many experimental studies have been conducted to ascertain the main chemical reactions and phase transformation condition in hydrothermal systems, such as the experimental study of alkali metasomatism and spilitization in closed system dominated by K^+, Na^+, Ca^{2+}, feldspar, mica and clay at 300–400°C and 200 MPa (Winkler and von Platen, 1961; Orville, 1962). Experimental studies were also conducted about hydrothermal alteration, with emphasis on hydrogen metasomatism and phase transformation of K-feldspar and albite in the Na_2O-K_2O-Al_2O_3-SiO_2-H_2O system at different conditions (Hemley, 1959; Hemley and Jones, 1964; Hemley et al., 1980; Sverjensky et al., 1991; Haselton et al., 1995). Phase stability field and boundaries of K-feldspar were also investigated in the KCl-HCl-H_2O system containing K-feldspar, muscovite, andalusite and quartz at 400–750°C and 40–80 MPa (Frank et al., 1998; Frank and Vaccaro, 2012).

These published studies focused mainly on the controlling factors of the multicomponent reactions and phase changes in a closed system, without considering the spatial gradient effect of species in the actual system. In reality, alteration-mineralization in porphyry deposits is controlled by a number of factors, and the ore-forming fluids migrate in specific direction accompanying the mass redistribution between the fluids and wall rocks. The local (sub)-equilibrium between the fluids and wall rocks is reached, gradually forming the alteration/mineralization zoning (Barnes, 1997). Therefore, the flow-reaction model resembles geometrically more the actual ore-forming environment, where a series of finite fluid batches successively react with the rock column. Consequently, a suite of distinct alteration fronts is formed when the fluids percolate through permeable rocks via infiltration or diffusion (Reed, 1997). The first application of flow-reaction model is to investigate water-rock metasomatism process (Korzhinskii, 1959, 1970) and stable isotope zonation (Bickle and Baker, 1990; Ferry and Dipple, 1991, 1992). Another application is about the effective Sn extraction from granite-related hydrothermal systems by comparing the results derived from a closed system and a flowing system. The results show that the maximum cassiterite ore grade was underestimated by almost an order of magnitude in the closed system than that in the flowing system, which underwent successive dissolution and precipitation processes. The cassiterite grade from the flowing system was also closer to the actual grade (Heinrich, 1990). Other application examples of flow-reaction model include the formation of sediment-hosted Cu deposits and magmatic-hydrothermal replacement deposits, shallow enrichment of porphyry Cu deposits by groundwater advection and the reaction of CO_2-rich brine with basalt in a flowing system (Merino et al., 1986; Holyland, 1987; Ague and Brimhall, 1989; Rogers et al., 2006; Luhmann et al., 2017). In this study, flow-reaction apparatus was applied to simulate the interactions of the ore fluids with common volcanic wall rocks (basaltic andesite) in porphyry Cu systems, in order to reveal the metasomatic process and elemental behavior during alteration, and to provide some preliminary exploration indicators. The initial fluid composition is based on LA-ICP-MS analysis results of individual fluid inclusions in the earliest high-temperature

(potassic) alteration zone of typical porphyry Cu deposits (Halter et al., 2002, Rusk et al., 2004, 2008; Heinrich, 2005; Landtwing et al., 2005, 2010).

2. Initial materials and experimental methods

2.1 Rock sample

The rock samples were collected from lower Carboniferous Qiershan Group in Eastern Tianshan Orogen, which are the main wall rocks of the Tuwu-Yandong porphyry Cu orebodies. The basaltic andesite samples are porphyritic, massive and dark-grey to black in color. The rocks are mainly composed of plagioclase (65 vol.%), clinopyroxene (10 vol.%), orthopyroxene (5 vol.%), groundmass (20 vol.%) and trace hematite (Figure 1). The rocks are weakly sericite-, argillic- and epidote-altered. The least-altered parts of the rocks (with no hydrothermal veins) were selected. The rock samples were crushed to about 1 cm and then soaked in 0.1mol L^{-1} HCl solution for 24 h to remove the impurities and altered components, and then rinsed with deionized water before dried. 50 g of the sample grains were grinded into powder (< 200 mesh) for major element oxide and trace element analyses. The remaining sample particles were milled into 40–60 mesh to ensure homogeneity and enhance reaction rate during the experiment.

2.2 Fluid sample

Compositional analysis of individual fluid inclusions is lacking for the Paleozoic Tuwu-Yandong porphyry Cu deposits, which display features of multistage mineralization and post-mineralization alteration (Xiao et al., 2015; Wang et al., 2016). Therefore, the initial fluid salinity and temperature used in this experiment are based on the conventional fluid inclusion microthermometric results of representative porphyry Cu deposits worldwide (Roedder, 1971; Nash, 1976; Heinrich, 2005). For instance, Nash (1976) have studied the fluid inclusions of 37 porphyry Cu deposits in United States and divided them into two main types, i.e., high-temperature, high-salinity fluid inclusions and intermediate-low temperature, low salinity fluid inclusions. Heinrich (2005) also classified fluid inclusions in porphyry Cu deposits into two main types according to the homogenization temperature and total salinity. These two different fluid inclusion clusters have similar ranges of salinity and homogenization temperature, i.e., a 2–20 wt.% ($NaCl_{eq}$) and 200–450°C cluster, and a 27–80 wt.% ($NaCl_{eq}$) and 300–800°C cluster. In this study, the experimental temperature and total salinity of the initial fluids are within the above ranges.

Chemical composition of the initial fluid is based on quantitative analysis results of individual fluid inclusions from high-temperature alteration zone in typical porphyry Cu deposits, such as those from the earliest ore-barren quartz veins in the Butte porphyry Cu-Mo deposit (Rusk et al., 2004, 2008), and those from the pre-main-stage quartz veinlets in the Bingham porphyry Cu-Mo-Au deposit (Landtwing et al., 2005, 2010). The components of these individual fluid inclusions approximate the composition of the primary fluid exsolved from the causative magma, with its major cations dominated by Na^+, K^+ and Cu^{2+}. There are also high Fe^{2+} and Ca^{2+} contents in the actual ore-forming fluid, but the addition of large amounts of Fe^{2+} and Ca^{2+} into the experimental fluid at room temperature have two problems. First, $CaSO_4$ is largely insoluble in SO_4^{2-}-rich fluid at room temperature, and hence the addition of Ca^{2+} would lead to $CaSO_4$ precipitation and decrease the initial fluid sulfate content significantly. Second, when large amount of Fe^{2+} ions are added to the initial fluid, the Fe^{2+} in the solution is destabilized and hydrolyzed readily over the long experimental period. LA-ICP-MS analysis of the liquid-phase fluid inclusions in Bingham showed that Mg^{2+} is another major cation in addition to Na^+, K^+ and Ca^{2+}. Therefore, Mg^{2+} was added to the experimental fluid as an important cation. Previous studies indicated that Ti^{4+}, Sr^{2+} and Pb^{2+} can be used as indicators of specific minerals in porphyry systems, and the correlation between the contents of these elements and the distance from the orebody can be used as a vectoring tool to locate the hydrothermal center(s) (Cooke et al., 2014a, 2017; Wilkinson et al., 2015). Therefore, a small amount of Ti^{4+}, Sr^{2+} and Pb^{2+} ions were also added into the initial fluid to reveal the distribution trend of these elements in the hydrothermal system, and to provide exploration implications according to their content variation in the wall rocks. Therefore, the main components of the initial fluid include Na^+, K^+, Cu^{2+}, Mg^{2+}, Cl^- and SO_4^{2-} and trace Ti^{4+}, Sr^{2+}, Pb^{2+} and NO_3^-, which approximately represents the actual ore-forming fluid. An equal amount of $Sr(NO_3)_2$ and $Pb(NO_3)_2$ was added into the initial fluid, while the Sr^{2+} and Pb^{2+} ions would form insoluble electrolytes with other ligands in the solution. The Sr^{2+} and Pb^{2+} concentrations were calculated using the corresponding solubility product constants at room temperature, yielding 1.0×10^{-6}–1.88×10^{-6} and 4.7×10^{-8}–9.4×10^{-8} mol L^{-1}, respectively (Table 1). The initial ex-

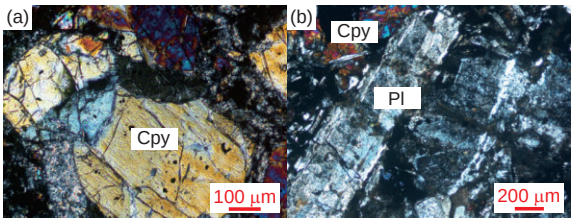

Figure 1 (Color online) Photomicrographs of the porphyritic basaltic andesite samples. Cpy, Clinopyroxene; Pl, Plagioclase.

Table 1 Major components of initial experimental fluid

Experimental temperature	Total fluid (mL)	Na^+ (mol L^{-1})	K^+ (mol L^{-1})	Cu^{2+} (mol L^{-1})	Mg^{2+} (mol L^{-1})	Ti^{4+} (mol L^{-1})	Cl^- (mol L^{-1})	SO_4^{2-} (mol L^{-1})
450°C	500	1.24	0.48	0.06	0.11	0.003	1.72	0.17
350°C	500	0.62	0.24	0.03	0.05	0.003	0.86	0.08

perimental fluid was made of analytical standard chemical reagent and deionized water. We attempted to remove oxygen by bubbling nitrogen into the deionized water for 3 hours before using.

2.3 Experimental apparatus and procedures

In general, the experimental simulation system for fluid-rock interactions can be divided into closed and open systems. The main application of a closed system is to determine the dominant chemical reactions that contribute to multi-component reaction and conditions of mineral phase transformation. It can also be used to determine the reaction rate and mechanism based on thermodynamic equilibrium and kinetic experiments (Brimhall, 1977; Bird et al., 1984; Hutcheon et al., 1993). The limitation of a closed system simulation is that the results could only imply element content variations and reaction process, without the consideration of spatial dimension in the geological processes. Another limitation is that setting too high the fluid/rock ratio in a closed system is not geologically realistic, as rock porosity in the crustal interior is usually below 10% by volume (Heinrich et al., 1996). However, the flow-reaction models consider the spatial dimension and direction of fluid flow, and are thus closer to the geological reality, where a batch of finite fluid successively percolates through a permeable rock column via infiltration or diffusion, and alteration fronts are formed. Therefore, the fluid-reaction models can provide a robust reflection of alteration process and spatial redistribution of elements (Carmichael, 1987; Lasaga and Rye, 1993).

This experiment was conducted using the flow-reaction instrument at the Lanzhou Center of Oil and Gas Resources, Chinese Academy of Sciences (CAS). This device can be regarded as a semi-open fluid flow system that contains three subsystems (Figure 2a), i.e., a high-temperature and high-pressure reaction system, a fluid collection and filling system, and experimental data recording system. The heating temperature range is 50–650°C and the maximum lithostatic and fluid pressures are 280 and 150 MPa, with accuracy of ±1°C, ±1 MPa and ±0.5 MPa, respectively. The sample cell is 14 cm in length and 2.5 cm in diameter, and can load a maximum of 150 g rock samples. The remaining space of the sample cell was filled with alloy pads after the sample loading (Figure 2b). The rock sample was compressed by lithostatic pressure at the upper side and withstood confinement pressure at the bottom side to balance the lithostatic pressure, and the sealing rings at both sides were simultaneously subjected to lithostatic and confinement pressure (Figure 2c). Under high temperature, the compressed sealing rings underwent plastic deformation to seal off the entire reactor. The alloy conduits connected to both ends of the autoclave are resistant to acid corrosion and are linked to solenoid valves and pressure transmitters that control fluid replenishment and discharge in the autoclave.

This experiment set two temperatures, 450 and 350°C, which are within the range of high-intermediate temperature alteration in porphyry Cu deposits (Bondar et al., 2014). The corresponding experimental lithostatic and fluid pressures are 110, 80, 45, 35 MPa respectively. According to the Airy isostasy model and assumed average upper crust density of 2.75 g cm^{-3} (Airy, 1855; Du, 2010), the burial depths corresponding to the experimental lithostatic pressure are 4.1 and 3 km, which agrees with the common porphyry Cu mineralization depths (<5 km) (Sillitoe, 2010). The lithostatic pressure represents the compaction of overlying rock formation above the alteration depth. The experimental fluid was filled in the pores of the rock samples and interacted with them. Fluid pressure was greater than the hydrostatic pressure of corresponding depth and is in accord with pressure of ore-forming fluid in porphyry Cu deposits derived from fluid inclusions measurement (Seedorff et al., 2005; Zhang et al., 2011). Therefore, the rock samples mainly received lithostatic pressure and surrounding fluid pressure during the experiment. This is similar to the actual scenario of wall rock compaction, with the widespread development of stockwork veins and/or breccias in porphyry Cu systems.

Before the experiments started, the rock samples were filled into the reaction cell and ran pressure system to seal off the reaction cell. The entire device was then vacuumed and checked for leakage. After the experiment started, the autoclave was heated up automatically at 10°C min^{-1}, and then slowed down to 2°C min^{-1} when the temperature gap from the set value was below 50°C. Once the target temperature was reached, fluid pressure and threshold value (±0.5 MPa) on high-pressure pump was set, and the experimental fluid was injected into the reaction cell at constant flux. When pressure value exceeded the threshold range, the outlet solenoid valve opened to discharge trace fluid to reduce pressure in the reaction cell to the target value. Therefore, fluid pressure in the cell was maintained at the target value during

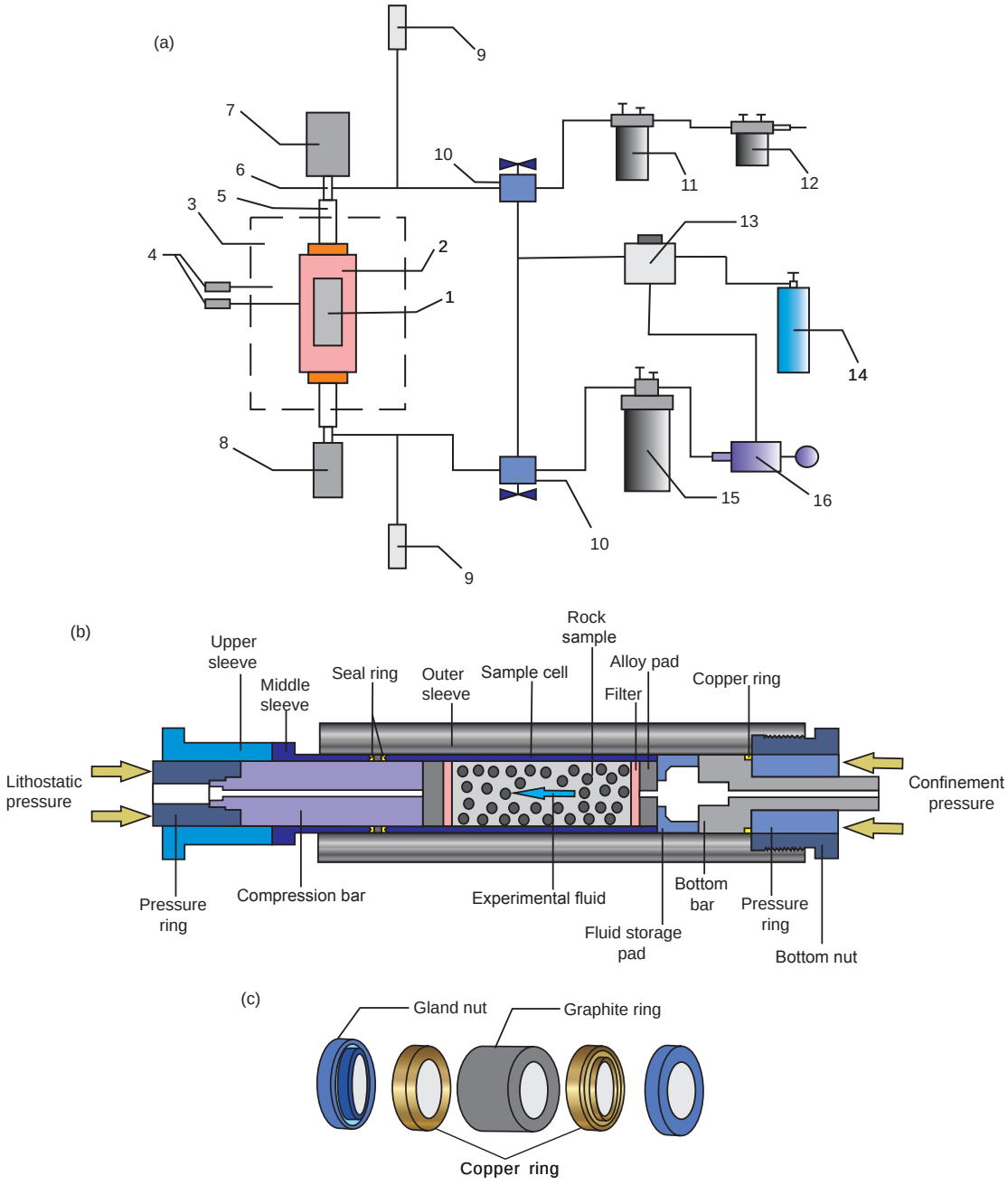

Figure 2 (Color online) Instrument used for the fluid-rock interaction experiment (a), nickel alloy reaction cell (b) and sealing rings (c). 1, Sample cell; 2, Autoclave; 3, Heating furnace; 4, Temperature transmitter; 5, Oil cylinder; 6, Compression bar; 7, Lithostatic pressure system; 8, Confinement pressure system; 9, Pressure transmitter; 10, Solenoid valve; 11, Cold trap; 12, Gas collector; 13, Air compression system; 14, Nitrogen gas; 15, Experimental fluid; 16, Fluid pressure control system.

the experiment. The experimental fluid discharged from the reactor flowed into a collector containing a cold trap and was sampled at constant 24-hour intervals. Experimental parameters, such as the temperature, pressure and initial heating rate, were controlled and recorded automatically by the software. After the experiment ended, the reactor was quickly cooled to room temperature and the rock column was removed. The fluid flow direction was marked on the columns for future analyses (Table 2).

The experimental rock columns (Figure 3a and 3c) were segmented along the fluid flow direction. The 450°C products were divided into three sections (Figure 3b), and the 350°C products were divided into two sections (Figure 3d). The divided products were broken equally into two parts. One half was crushed into grains, rinsed with deionized water to clean and dried, and then grinded into powder (<200 mesh) for composition analysis. The other half was solidified with resin and made into thin section for micrographic ob-

Table 2 Experimental temperature and pressure conditions and parameters

Experiment	Temperature (°C)	Lithostatic pressure (MPa)	Fluid pressure (MPa)	Rock mass (g)	Sample size (mesh)	Salinity (wt.%) ($NaCl_{eq}$)	Duration (h)	Collecting frequency (h/time)	Single fluid volume (mL)
01	450	110	45	70.0	40–60	12.8	385	24	28
02	350	80	35	36.5	40–60	6.9	410	24	15

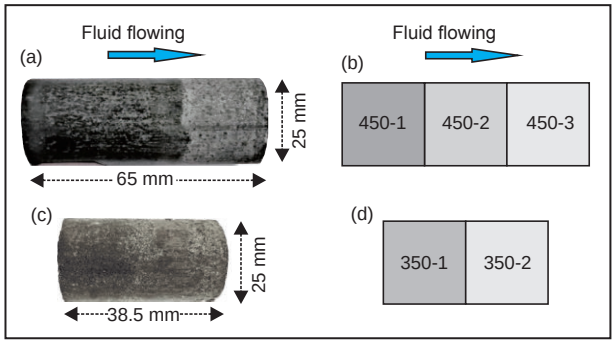

Figure 3 (Color online) Columnar experimental products and divided segments. (a), (b) 450°C products; (c), (d) 350°C products.

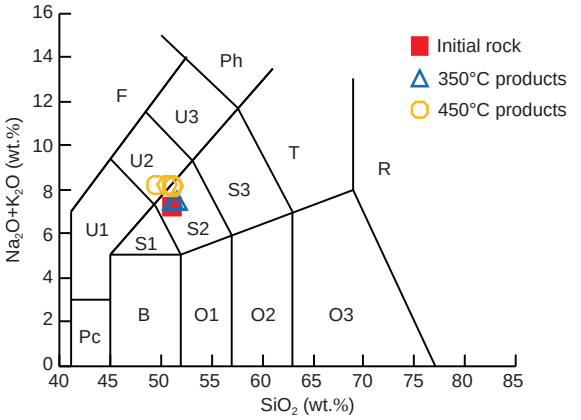

Figure 4 (Color online) Total alkali vs. SiO_2 diagram of initial rock and experimental products. B, basalt; O_1, basaltic andesite: O_2, andesite; O_3, dacite; R, rhyolite; S_1, trachybasalt; S_2, basaltic trachyandesite; S_3, trachyandesite; T, trachyte-trachydacite; Pc, picro-basalt; U_1, tephrite-basanite; U_2, phonotephrite; U_3, tephriphonolite; P_h, phonolite; F, foidite.

servation and electron probe microanalysis (EPMA). These procedures were completed without contamination.

2.4 Whole-rock geochemical and EPMA analyses

Major element analyses were conducted with X-ray Fluorescence (XRF) at ALS Chemex (Guangzhou) Co. Ltd., and the accuracy is better than 1%. Trace element compositions were analyzed using a Thermo iCAP Qc (ICP-MS) at State Key Laboratory of Isotope Geochemistry of the Guangzhou Institute of Geochemistry, Chinese Academy of Sciences (GIGCAS). The analysis accuracy is better than 3% for rare earth elements (REEs) and 5% for other trace elements. Analysis procedures follow the ones described in Liu et al. (1996).

Major oxides of mineral phases were analyzed using a JEOL150 JXA-8230 EPMA at the Key Laboratory of Mineralogy and Metallogeny of GIGCAS. The operating conditions were 15 kV accelerate voltage, 20 nA probe current and 1 μm beam size. The relative precision is better than 0.01% for all elements and natural crystal standards were used.

3. Results

3.1 Chemical composition of experimental products

In the TAS diagram, the 350°C products are similar to pristine rocks, and are plotted in the basaltic trachyandesite field. The 450°C products were changed from basaltic trachyandesite to phonotephrite, probably by hydrothermal alteration (Figure 4). Total alkali content in the experimental products is higher than that of pristine rock, a phenomenon that becomes more obvious with increasing temperature. The K_2O/Na_2O ratio of experimental products also varies: 1.24 (pristine rocks), 1.21–1.22 (350°C products) and 1.43–1.72 (450°C products). At the upstream of experimental rock column (along fluid flow), the SiO_2 content of all products decreases, especially for the 450°C products.

The pristine rocks and experimental products display similar trace element variation characteristics (Figure 5a). Large-ion lithophile elements (LILEs) such as Rb, Ba, K, and Sr are enriched, while high-field strength elements (HFSEs) such as Th, Nb, Ta, Zr, Hf and Ti are depleted, all indicating arc-type geochemical affinity. The experimental products also exhibit consistent chondrite-normalized REE patterns (Figure 5b), where LREEs are slightly enriched and HREEs are relatively depleted. The total REE contents gradually decrease from pristine rocks to products with increasing temperature. The average contents of total REE are 136 ppm (1 ppm=1 mg L^{-1}) (pristine rocks), 132 ppm (350°C products) (Table 3) and 129 ppm (450°C products).

3.2 Element spatial distribution in experimental products

Analysis results of major elements in the same experimental

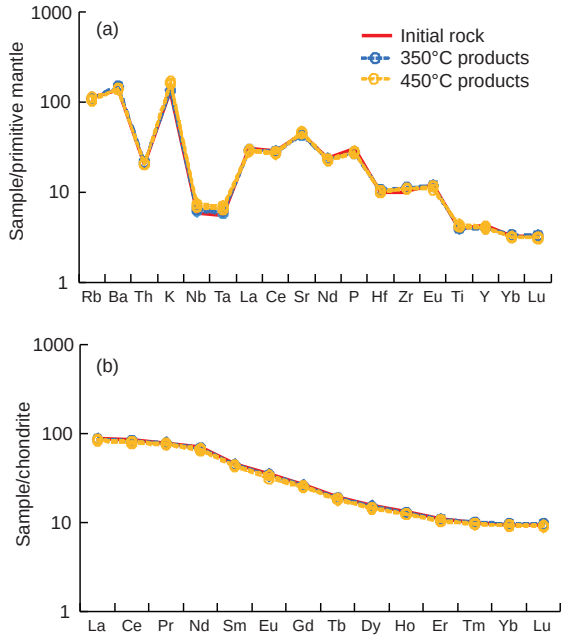

Figure 5 (Color online) Primitive mantle-normalized multi-element spidergram (a), chondrite-normalized REE distribution patterns (b). Normalization values are from Sun and McDonough (1989).

product show heterogeneous redistribution trends and variation of elements during the fluid-rock interactions. The same element also shows disparate variation trends under different experimental temperatures. For instance, the degree of variation is greater in the 450°C products than in the 350°C ones, which implies that higher temperature may have significant effect on elemental redistribution in hydrothermal systems. Contents of CaO and MgO all decrease in experimental products, but they display different variation trends along the fluid flow direction (Figure 6c and 6d). Along the fluid flow direction, leaching of CaO gradually weakens but leaching of MgO strengthens. In contrast, K_2O and TiO_2 contents increase in all experimental products, particularly in the 450°C ones (Figure 6a and 6f) but the enrichment is gradually reducing along the fluid flow. Na_2O content increases weakly in the 350°C products, while that decrease at upstream and increase at downstream in the 450°C products (Figure 6b). SiO_2 content also decreases at upstream and increases at downstream in all the products, but the enrichment is more significant in the 350°C products (Figure 6e). All major element oxide contents, except for MgO, show the greatest variation at upstream (450-1) in the 450°C products, but this trend is not apparent in the 350°C ones.

Trace elements, such as Cu, Zn, Mn, Sr, Pb and S, are most affected by water-rock interactions, and have different degree of variation under different experimental conditions. The variation of these elements in the 450°C products is greater than that in the 350°C ones, which implies that higher temperature may play a crucial role in causing elemental enrichment or depletion. Both Cu and S are distinctly enriched in all the products, and the enrichment reaches a maximum at upstream (Figure 7a and 7b), whereas Cu and S contents decrease rapidly along the fluid flow, especially under higher temperatures. Zinc and Mn contents decrease in all the products, especially under high temperatures (Figure 7c and 7d). Along the fluid flow direction, the leaching is almost invariable for Mn, but Zn has different leaching trends under different conditions, and the leaching gradually strengthen and weaken in the 450 and 350°C experimental products, respectively. Strontium content increases slightly in the 450°C products and decreases in the 350°C ones (Figure 7e). Lead content increases at upstream and decreases at downstream in the 450°C products, but stays constant in the 350°C ones (Figure 7f).

3.3 EPMA results

Major element oxide contents in the minerals from the pristine and experimental rocks were determined, such as pyroxene, feldspar and epidote, and the analysis spots were distributed from core to rim in these minerals (Figure 8). Analysis results indicate that mineral composition is homogeneous from core to rim in pristine rocks (Figure 9a–f). Therefore, the fluid-rock interaction processes can be revealed by comparing the compositional variation of minerals from core to rim.

Chemical composition proximal to the mineral core is mostly constant, but the composition varies distinctly and H_2O content increases at the mineral margin in the experimental products. TiO_2 content is almost constant from mineral core to rim in the 350°C products, but it decreases at the pyroxene rim and clearly increases at the rim of epidote and feldspar in the 450°C ones (Figure 10a and b). CaO content decreases markedly at the rim of bytownite, epidote and pyroxene in all the products, while it has no clear decrease at the oligoclase rim due to its low original CaO content (Figure 10c and 10d).

K_2O content decreases at oligoclase rim and slightly increase at the rim of epidote and pyroxene in 350°C products. However, K_2O content increases significantly at the rim of all minerals in the 450°C products (Figure 11a and 11b). Na_2O content increases at the epidote rim and slightly decreases or remains constant at the rim of feldspar and pyroxene in all the products (Figure 11c and 11d). SiO_2 and Al_2O_3 contents decrease at the rim of feldspar (esp. oligoclase) and epidote, and have no apparent variation at the pyroxene rim in the 450°C products (Figure 12a and 12b).

4. Discussion

4.1 Silicic alteration process in experimental system

Experimental results show that compositions of the experi-

Table 3 The Composition of initial rock and experimental products

Major elements (wt.%)	Initial rock	350-1	350-2	450-1	450-2	450-3
Al_2O_3	17.34	17.51	17.70	17.20	17.48	17.52
BaO	0.10	0.11	0.12	0.11	0.12	0.12
CaO	6.25	5.66	5.71	5.00	5.54	5.68
TFe_2O_3	9.20	9.20	9.17	10.64	9.17	9.01
K_2O	3.92	3.96	4.01	5.05	4.77	4.67
MgO	5.88	5.50	5.48	5.46	5.35	5.34
MnO	0.14	0.13	0.13	0.10	0.11	0.11
Na_2O	3.15	3.28	3.30	2.93	3.27	3.26
P_2O_5	0.48	0.43	0.42	0.42	0.44	0.44
SiO_2	49.85	49.37	50.28	48.26	49.95	49.87
SO_3	0.02	0.11	0.05	0.95	0.39	0.16
SrO	0.11	0.10	0.10	0.11	0.11	0.11
TiO_2	1.14	1.15	1.15	1.27	1.21	1.20
LOI	2.71	2.93	2.63	3.02	2.56	2.41
Total	100.29	99.44	100.25	100.52	100.47	99.90
Minor elements (ppm)	Initial rock	350-1	350-2	450-1	450-2	450-3
Rb	72.70	69.08	71.06	72.20	67.24	65.75
Ba	970.40	1017.40	1065.10	965.90	990.10	982.40
Th	1.74	1.82	1.85	1.76	1.77	1.73
Nb	4.14	4.38	4.61	4.44	4.68	4.93
Ta	0.23	0.24	0.25	0.24	0.26	0.27
Sr	940.50	903.70	930.90	967.50	949.60	991.20
Hf	3.07	3.15	3.32	3.18	3.22	3.08
Zr	114.60	124.50	126.60	124.60	122.50	121.80
U	0.58	0.58	0.62	0.56	0.57	0.56
Y	19.48	18.08	18.43	19.03	17.90	18.47
Cu	70.72	368.40	180.20	1846.60	750.60	560.50
Mn	1063.40	976.10	988.30	797.30	816.70	815.30
Zn	105.00	93.03	99.00	77.79	78.94	72.24
Sr	940.50	903.70	930.90	967.50	949.60	991.20
Pb	7.88	8.25	7.84	20.92	32.44	25.60
La	20.86	20.09	20.68	19.47	20.39	20.16
Ce	51.48	49.15	50.71	47.30	49.24	49.57
Pr	7.43	7.19	7.48	7.06	7.35	7.23
Nd	32.75	30.91	32.00	30.03	31.52	31.03
Sm	6.93	6.66	6.85	6.46	6.67	6.65
Eu	2.02	1.94	2.01	1.79	1.95	1.95
Gd	5.46	5.18	5.37	5.03	5.26	5.15
Tb	0.73	0.69	0.71	0.67	0.69	0.69
Dy	3.89	3.69	3.87	3.60	3.74	3.66
Ho	0.74	0.71	0.73	0.69	0.70	0.71
Er	1.82	1.73	1.80	1.68	1.75	1.74
Tm	0.26	0.25	0.26	0.24	0.25	0.25
Yb	1.59	1.57	1.65	1.54	1.57	1.58
Lu	0.23	0.24	0.25	0.23	0.23	0.23
∑REE	136.18	130.00	134.35	125.78	131.31	130.58
La/Yb	13.09	12.76	12.53	12.63	12.98	12.77
δEu	0.97	0.97	0.98	0.93	0.97	0.98

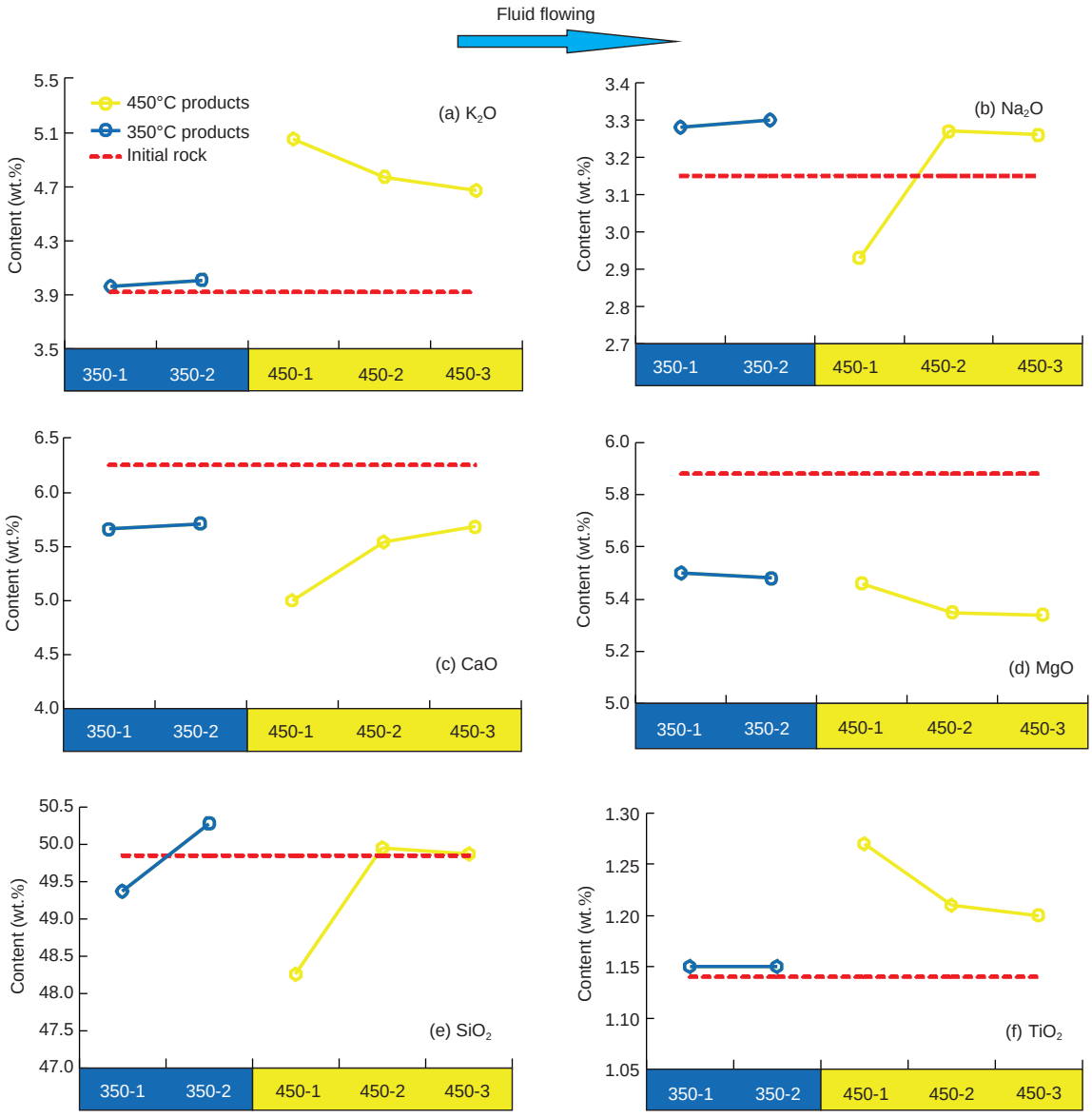

Figure 6 (Color online) Variation trends of major element contents in experimental products along the fluid flow direction.

mental products change significantly comparing to those of the pristine rocks, and that the compositions of mineral rim are also more variable than those of mineral core, which implies the occurrence fluid-rock interactions (i.e., alteration) in the experimental system. Previous experimental studies suggested that hydrothermal replacement of rocks comprises interface reaction and mass transport (Zhang, 2010). Fluid-silicate mineral interactions are mainly controlled by interface reactions, and involves (i) absorption of H^+, (ii) ionic exchange and (iii) cation desorption at the mineral-fluid interface. The ionic exchange process is affected by the types of chemical bonds, H^+ concentrations and activation energy of the reactions (Murphy et al., 1989; Tan et al., 1994; Schott et al., 2009). The chemical bonds formed by various elements have distinct bond energy, and thus causes nonstoichiometric dissolution of elements in the mineral lattice during metasomatic process (Wang et al., 2000; Schott et al., 2009).

According to previous research, the reactions at the fluid-silicate interface involve a series of ions substitution processes in the mineral lattice, and eventually lead to modification or destruction of the silicate structure (Oelkers et al., 1994). The dissolution of silicate/oxide minerals, as indicated by previous dissolution experiments of basaltic glass, K-feldspar, albite, and pyroxene (Gautier et al., 1994; Oelkers, 2001; Gislason and Oelkers, 2003), includes three major processes: (i) univariant/divalent cations on the mineral surface are removed through cationic exchange; (ii) aluminum from the mineral lattice is released by exchange reactions; (iii) slow liberation of Si and the silicate structure is gradually destroyed (Oelkers, 2001).

The Si-O bond tends to become polar covalent bond and

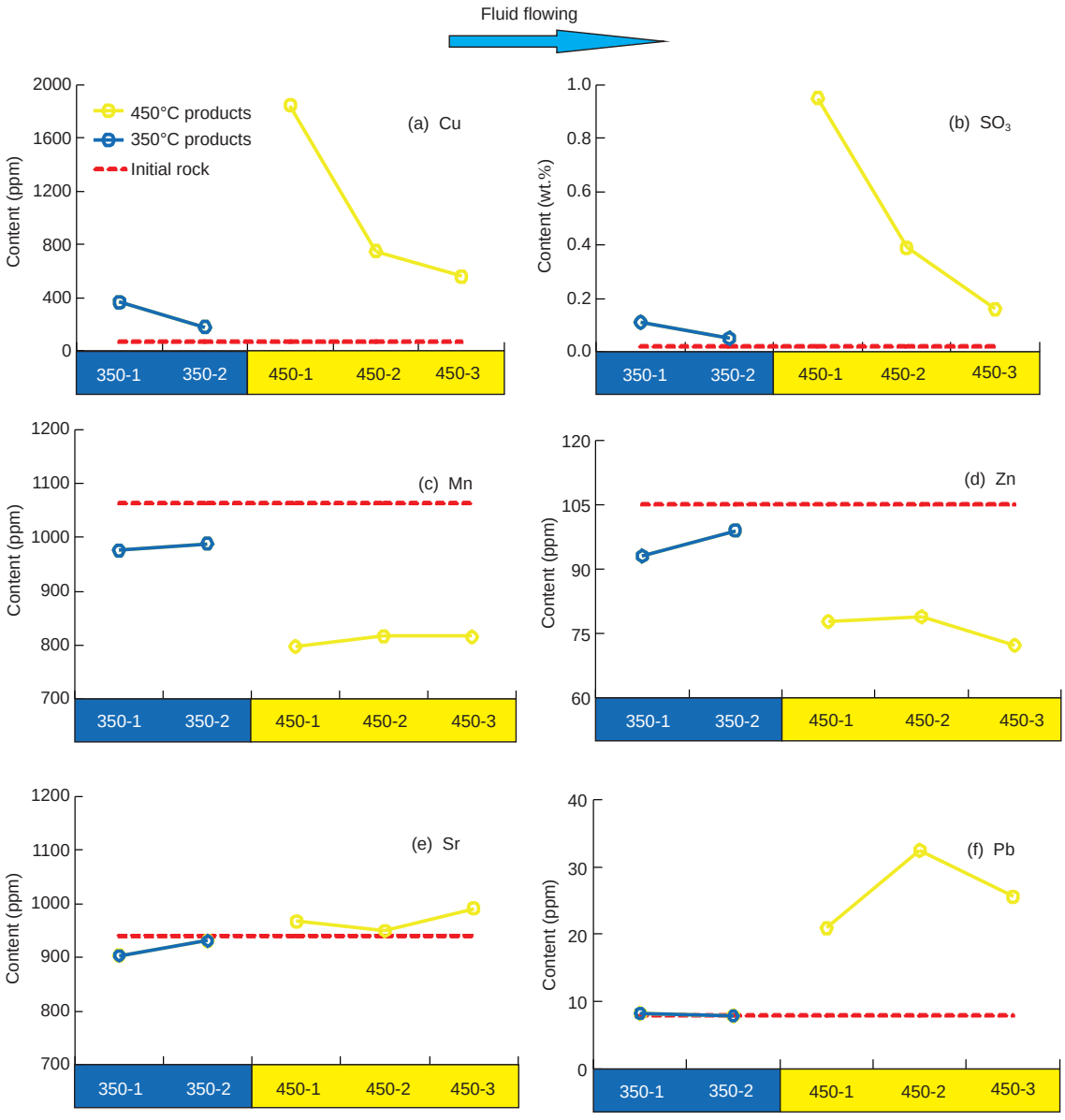

Figure 7 (Color online) Minor elemental variation trends in experimental products along the fluid flow direction.

the physicochemical properties of water will be changed at above 300°C, which contributes to the breakage of hydrogen bond, hydration of substance containing polar covalent bond and eventually the leaching of Si (Huang et al., 2011). Our experimental results indicate Si leaching, especially in the 450°C products. The Si and Al contents at the rim of bytownite and epidote also decrease. The mol_{Si}/mol_{Al} ratio increase form core to rim, i.e., from 3.32 to 32.54 (bytownite) and from 2.83 to 5.26 (epidote). This shows that the leaching of Al is more significant than Si in these two minerals (Figure 13a and b). Previous dissolution experiments of basaltic glass and silicate minerals show that the content of Al and Si leaching has good linear relationship in low temperature (<100°C) acidic solution, which implies that these two elements have a close liberation relation. The most possible dissolution mechanism is the leaching of Al that breaks the Si-O bond adjoining the exchanged Al site and lead to further Si leaching (Oelkers et al., 1994, 2001). However, the content of Al and Si leaching at the rim of bytownite and epidote in the experimental products has no clear linear relationship (Figure 13a and 13b), which indicates that the leaching of Al and Si may be affected by other factors, such as salinity and solution chemistry, in addition to temperature and pH in porphyry Cu fluid systems.

The fluid-rock interaction mechanism in this experimental system can be revealed based on the variation scale of elemental content in the experimental products coupled with previous experimental studies in a simple system (Oelkers et al., 1994; Oelkers and Schott, 2001; Gislason and Oelkers, 2003). In this process, the ions and alkali metals in the fluid

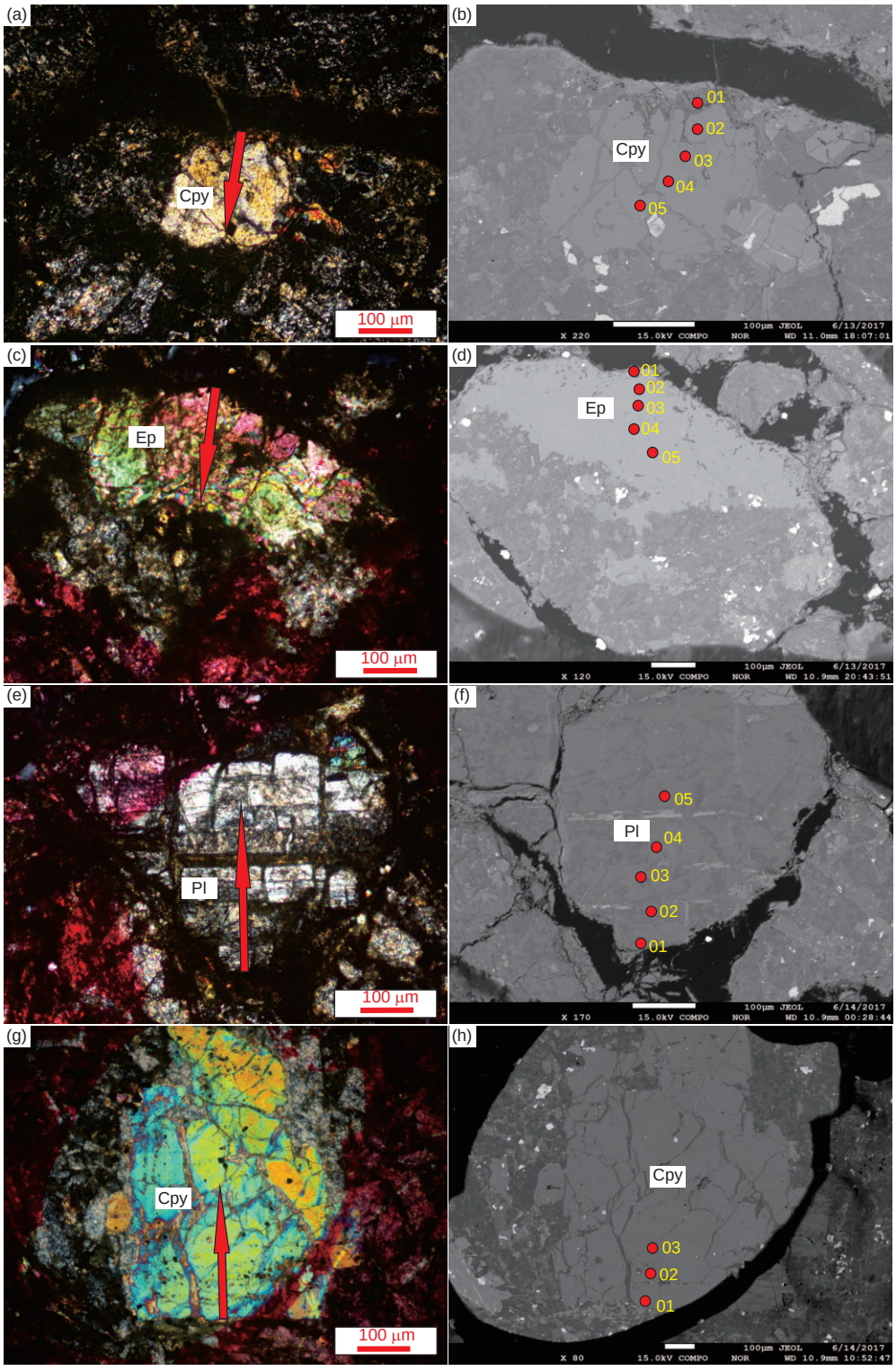

Figure 8 (Color online) Photomicrographs (left) and BSE images (right) of experimental products ((a)–(f)) and initial rock ((g), (h)). Red dots represent EPMA analysis spots and red arrows represent analysis direction. Cpy, clinopyroxene; Pl, plagioclase; Ep, epidote.

substitute selectively for cations in the mineral lattice. Monovalent and divalent cations are more easily leached, followed by Al and Si, which gradually alters the mineral structure (Figure 14a and 14b). According to the transition state theory, high temperature can increase the number of activated molecules, and therefore the elemental exchange reactions are more intense under higher temperature (Aagaard and Helgeson, 1982), which results in the more significant elemental enrichment or depletion in the 450°C products comparing to the 350°C ones.

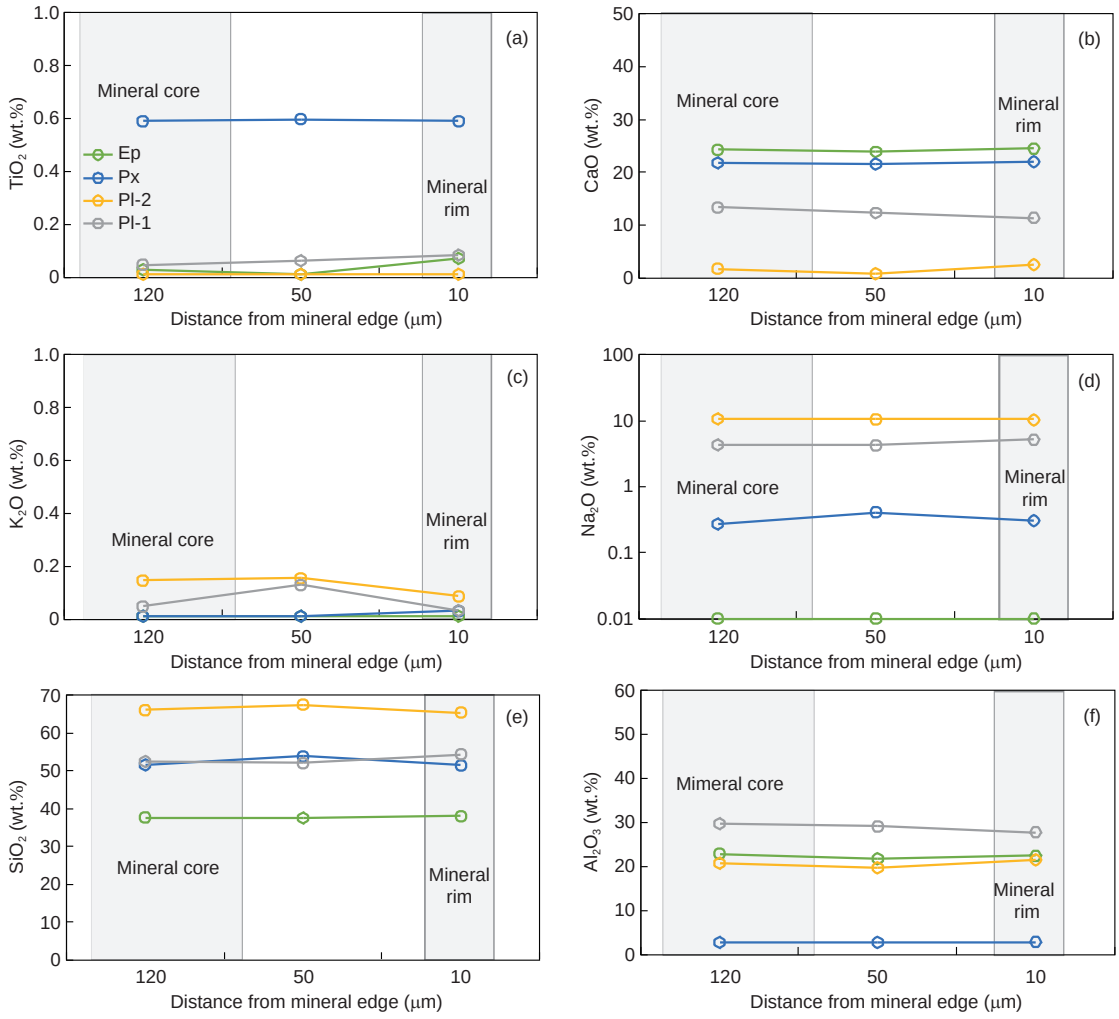

Figure 9 (Color online) Major element oxides of minerals in initial rock. Pl-1, bytownite; Pl-2, oligoclase; Px, pyroxene; Ep, epidote.

By comparing the elemental contents in the experimental products with those in the pristine rocks, the elemental mobility and transfer trend in the experimental system can be determined. This is achieved by performing integral calculation for element content variation in the experimental products, and then divided the values by the length of the columnar products. The final values are used to evaluate the elemental transfer trends and mobility. Elemental mobility of the leached elements (in decreasing order) is Ca, Mg, Si, Al, Mn and Zn. These elements preferentially enter the mineral lattice, with their (decreasing) order of substitution ability being K, Na, Ti, Sr and Pb. Previous experimental studies of the basalt-brine (seawater) system also showed non-stoichiometric dissolution of elements in the solid phase, among which univalent and bivalent elements are more active than Al and Si. However, the previous experimental results of Ca-K-Si-Al decrease and Na-Mg increase in the solid phase contradict with what were observed in typical porphyry Cu systems (Mottl and Holland, 1978; Dang and Hou, 1995; Liu and Zhang, 1996; Hu et al., 2010; Gudbrandsson et al., 2011).

4.2 Mechanism of potassic and albitic alterations in porphyry Cu system

Potassic alteration zone usually occur in the core of porphyry Cu systems, and is caused by high intermediate temperature metasomatism of magmatic fluid in the intrusion apex the wall rocks around it. The homogenization temperatures of fluid inclusion in the potassic zone commonly range from 250 to ≥600°C, mostly reaching 400°C (Sillitoe, 2010; Bondar et al., 2014). Although the mineral assemblage is slightly different in mafic to felsic country rocks, the main assemblage is dominated by quartz, K-feldspar, biotite, anhydrite, magnetite and Cu-Fe sulfides (Sillitoe, 1973, 2010). In many world-class porphyry deposits, the potassic zone hosts the bulk of the ores, such as the Bingham Cu deposit, where the most intensely potassic-altered rocks contain the highest ore grade (Redmond et al, 2004; Redmond and Einaudi, 2010; Landtwing et al., 2010). Therefore, it is ne-

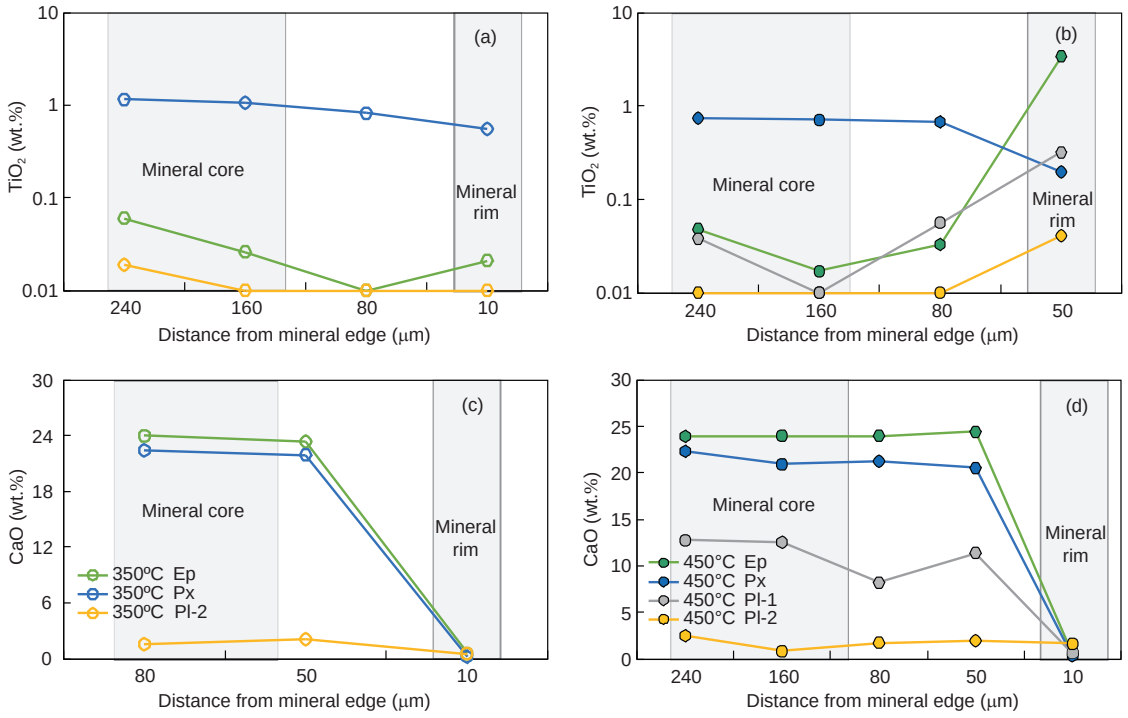

Figure 10 (Color online) TiO_2 and CaO content variation of minerals in ((a), (c)) 350°C and ((b), (d)) 450°C experimental products. Pl-1, bytownite; Pl-2, oligoclase; Px, pyroxene; Ep, epidote.

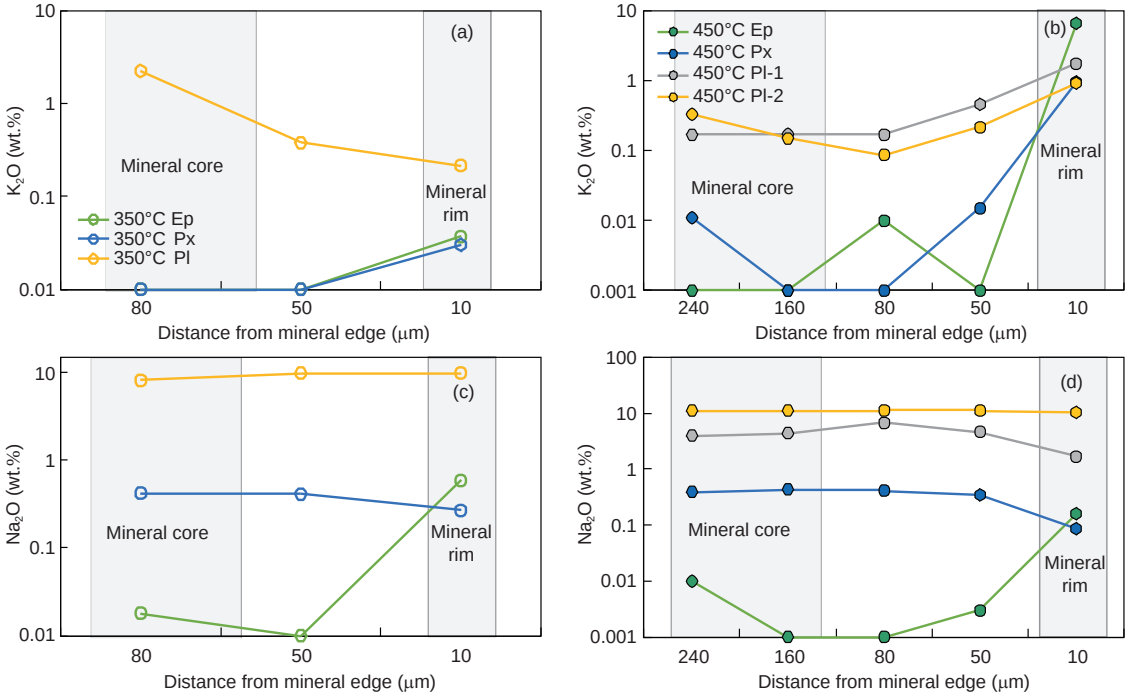

Figure 11 (Color online) K_2O and Na_2O content variation of minerals in ((a), (c)) 350°C and ((b), (d)) 450°C experimental products. Pl-1, bytownite; Pl-2, oligoclase; Px, pyroxene; Ep, epidote.

cessary to investigate the formation mechanism and porphyry Cu metallogenic role of potassic alteration. Many experimental studies were conducted to constrain the mechanism and controlling factors of high-temperature alteration by analyzing the elemental behavior, minerals composition variation and phase transition boundaries in the closed system (Hemley, 1959; Montoya and Hemley, 1975; Sverjensky et al., 1991; Haselton et al., 1995). Published

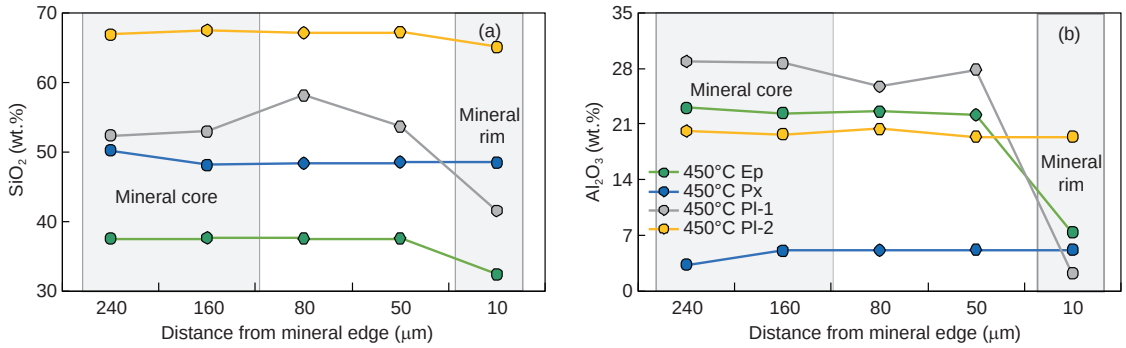

Figure 12 (Color online) Mineral SiO_2 and Al_2O_3 content variation in 450°C experimental products. Pl-1, bytownite; Pl-2, oligoclase; Px, pyroxene; Ep, epidote.

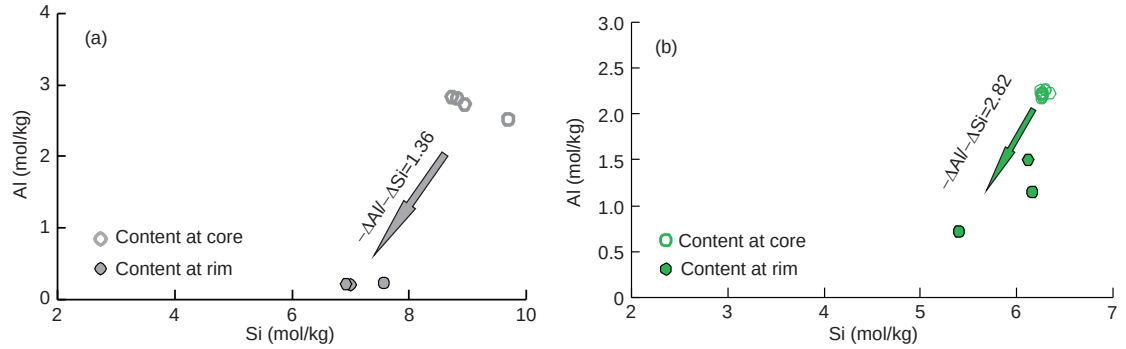

Figure 13 (Color online) Si and Al content of (a) bytownite and (b) epidote from core to rim. –ΔSi and –ΔAl represents leaching content of Si and Al at mineral rim.

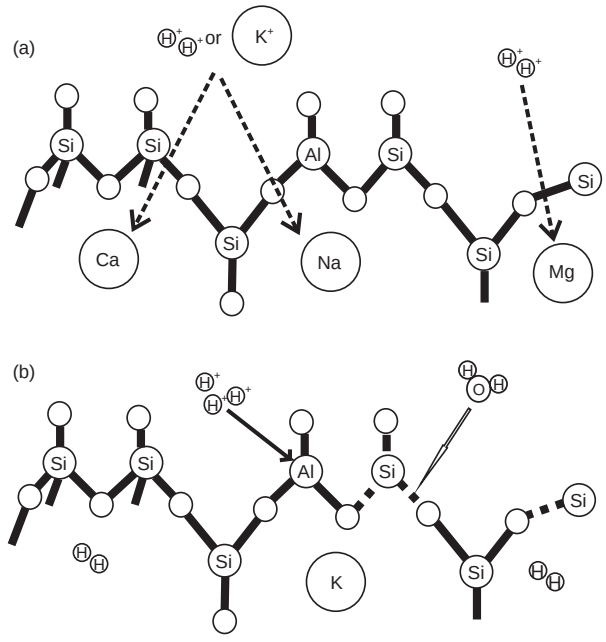

Figure 14 Mechanism of replacement of fluid with silicate in experimental system. (a) H^+ and K^+ exchange for monovalent and divalent cations; (b) H^+ exchange for Al and Si leaching. Modified after Oelkers and Schott (2001).

results indicate that the higher temperature and K^+/H^+ ratio in the fluids contribute to the stability of K-feldspar and potassic alteration, and similar variation trends can also be applied to albitic alteration under higher temperature and Na^+/H^+ conditions (Hemley and Jones, 1964; Frank et al., 1998; Frank and Vaccaro, 2012). However, there are few detailed studies about the effect of temperature, K^+ and Na^+ concentrations on potassic and albitic alterations in a flowing system.

The initial experimental fluid has the same K^+/Na^+ ratio, and can be used to investigate the relationship of potassic and albitic alteration under different temperatures. Analysis results show that total K_2O content increases significantly in the 450°C products, and has also an apparent increase at mineral rim (cf. mineral core), which all implies that the 450°C products were potassic-altered. The K_2O content in the 350°C products and that at the minerals rim vary gently with respect to the 450°C ones, which indicates high temperature may be the key controlling factor of potassic alteration. Along the fluid flow direction, potassic alteration at upstream causes the K^+ decrease, and further weaken potassic alteration at downstream. The increased K_2O content in the 450°C products is nearly 30 times of that in the 350°C ones, but the K^+ concentration of the initial fluid at the 450°C

experiment is only twice than that in the 350°C one. Moreover, the fluid-rock ratio is nearly the same in both experiments. Therefore, we can conclude that the temperature may be the main controlling factor for potassic alteration. The fluid inclusion microthermometric results also show that high temperature conditions are more favorable for potassic alteration in porphyry Cu systems (Sillitoe, 2010).

Na_2O content has distinct variation trends in different experimental conditions. Na_2O is leached at upstream and slightly enriched at downstream in the 450°C products, but it is mildly enriched in all the 350°C products. Previous experimental studies demonstrated that higher temperature and Na^+/H^+ ratios are favorable to albite alteration (Hemley and Jones, 1964). However, our results show that Na_2O content increase mildly in all experimental products, and imply that such experimental temperature condition does not favor sodic alteration. Na^+ concentration in the 450°C initial fluid is higher than that in the 350°C one, but that did not cause more intense sodic alteration in the 450°C experiment and the Na_2O increase in both products is approximately the same. This contrasts with the published experimental studies (Hemley and Jones, 1964). Comparing the Na^+ concentrations in the initial fluid and experimental (450 and 350°C) products, we suggest that higher fluid Na^+ concentrations are required to form the similar degree of sodic alteration at higher temperatures. In other words, it is more difficult to form sodic alteration at higher temperatures when the other fluid physicochemical parameters are held constant.

The reason for the different K_2O and Na_2O content variations in experimental products may be due to the fact that K^+ and Na^+ competitively replace each other or the same cation in the experimental system, and the incompatibility of these two elements in the same system leads to their different replacement trends (Du, 1986). K^+ enter preferentially into the silicate crystal lattice to replace cations under higher temperature (450°C) and leads to dominance of potassic over sodic alteration. However, it is more difficult for K^+ to enter crystal lattice under lower temperature (350°C), thus more Na^+ can enter the silicates and the same extent of sodic alteration is formed under different Na^+ concentrations. From the 350 to 450°C experiment, the Na^+ content of the initial fluid increases and is higher than the fluid K^+ content (mol_{Na+}/mol_{K+} ratio of all the initial fluid is 2.6). However, the K_2O content increase in the 450°C products is higher than that in the 350°C products by one order of magnitude, which implies that the potassic alteration is dominant under high temperature even though the fluid contains higher Na^+ concentration than K^+. As a direct product of magmatic-hydrothermal evolution, porphyry Cu mineralization generally develops potassic alteration in the core but sodic alteration is usually poorly preserved (Sillitoe, 2010). Our experimental results confirm this observation that the Na^+ exchange (and thus sodic alteration) would be significantly inhibited when the system have a certain amount of K^+, which may cause the absence of sodic alteration in porphyry systems.

However, it is noteworthy that sodic-calcic alteration is preserved at depths in some porphyry Cu systems, e.g., Yerington and Pebble (Carten, 1986; Seedorff et al., 2008). In general, these two types of alteration are formed simultaneously, but sodic-calcic alteration is distributed below the potassic alteration and is closer to the root zones of porphyry systems. The fluid that formed potassic and sodic-calcic alteration may have distinct thermodynamic properties and evolution paths due to their different formation depths. Therefore, we consider that the formation of sodic-calcic alteration is also controlled by the fluid (esp. for low K^+ ones) physiochemical properties and evolution paths. According to Pollard (2001), when the fluids unmixed through cooling or decompression, the Na/(Na+K) ratio in the CO_3^{2-}-bearing fluid is more likely to increase relative to the Cl^--bearing fluid, which contributes to wall rock albitization. High CO_2-fluid may cause significant sodic alteration by fluid unmixing, but the fluid CO_2 content in typical porphyry mineral systems is always low and thus sodic alteration is uncommon.

4.3 Element transport and contribution to mineralization

4.3.1 Non-mineralization-related elements

The experimental results indicate that CaO is significantly leached in all the experimental products, especially in the 450°C ones, and CaO content at the rim of bytownita, pyroxene and epidote also decreases, which implies high temperature is important for CaO leaching. Fluid inclusions from the different alteration zones in the Butte porphyry Cu-Mo deposit were analyzed using LA-ICP-MS. The main components in the earliest veins can approximately represent the composition of exsolved parental magmatic fluid, and the Ca content is below the detection limit. However, fluid inclusion Ca content in late pyrite-quartz veins is above the detection limit (Rusk et al., 2004), which indicates a Ca increase with fluid evolution. The increased Ca may be derived from the wall rock leaching by high-temperature fluid, as supported by our experimental results. The leached Ca could form Ca-rich minerals and anhydrite crystals were found in pores of the 450°C products (Figure 15a). Some porphyry Cu systems contain anhydrite (veins) in their potassic alteration zones, which indicates high oxygen fugacity of the ore-forming fluids (Yang et al., 2009; Cooke et al., 2014b; Chang et al., 2018). The presence of anhydrite in the ore-causative intrusions was also regarded as a direct indicator of oxidized magma (Stern et al., 2007; Liang et al., 2009), however this experiment shows that anhydrite can also be formed by Ca leaching and reprecipitation during potassic alteration, particularly when the fluid Ca content is relative low. Therefore,

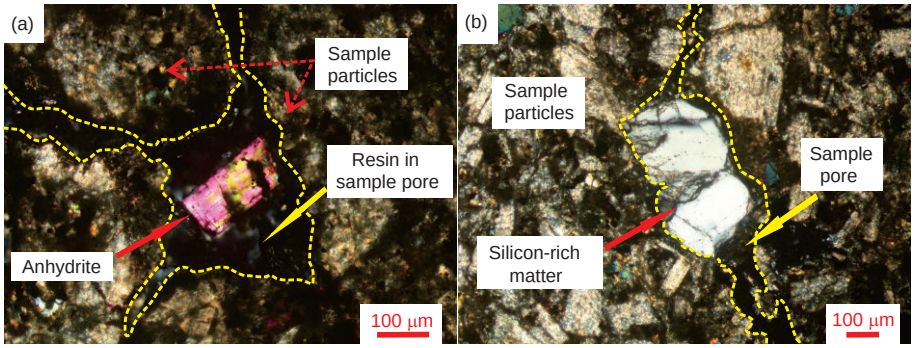

Figure 15 (Color online) Anhydrite in the 450°C experimental products (a) and SiO_2-rich material in the 350°C experimental products (b). Pore of sample particles is filled with resin.

anhydrite in the intrusions does not necessarily represent high oxygen fugacity of magma, and attention should be paid to distinguish primary anhydrite from secondary one.

MgO is leached in all products and the decrease of MgO content is more significant in the 450°C ones. Along the fluid flow direction, the leaching of MgO gradually strengthens, but the leaching of CaO gradually weakens. The reason may be that with the continuous leaching of Mg and Ca, their concentration in the fluid gradually increased and the higher Ca^{2+} concentration would inhibit further Ca leaching, whereas the increasing fluid Mg^{2+} concentration effect on further Mg leaching is subtle due to the high Mg^{2+}solubility in the Cl^--rich system (Liu, 1984). This experiment results revealed the possible formation process of propylitic alteration zone which extends laterally for several kilometers away from the coeval potassic alteration core and where abundant Mg-rich and Ca-rich minerals are developed, especially with mafic wall rocks (Sillitoe, 2010). We propose that CaO and MgO are both leached from the wall rocks into high-temperature fluid and when the fluid temperature decreases, the ability of transporting Ca^{2+} and Mg^{2+} would be weakened immensely and the distal propylitic alteration zone is formed.

Similarly, SiO_2 is also leached at upstream in all experimental products, especially under high temperature. Along the fluid flow direction, the leached SiO_2 precipitated and concentrated at downstream in the 350°C products (Figure 15b) while precipitated SiO_2 in the 450°C ones is unobvious. This indicates that high temperature is important for SiO_2 dissolution, and SiO_2 is more prone to leaching and transport at high temperature, and more likely to be precipitated at low temperature. Previous experimental studies suggested that quartz solubility in water decreases with temperature increasing at 300–500°C and 20–80 MPa (Fournier and Marshall, 1983; Fournier, 1999). Nonetheless, SiO_2 leaching is more obvious in the 450°C products, which indicates higher temperature and salinity fluid is more efficient for SiO_2 leaching and complex silicates may have different dissolution mechanism from quartz in water. The ore-forming fluid exsolved from magma has high temperature and its strong leaching ability may decrease the Si content in wall rocks. With the fluid migrates outward, the fluid SiO_2 content approaches saturation. As the fluid gradually cools, SiO_2 precipitates in the periphery of the hydrothermal system, where quartz-rich veins are widely developed.

Experimental results show that the TiO_2 content increase in the 450°C products is clearly higher than that in the 350°C ones and EPMA results also show that the TiO_2 content increase at mineral rim in the 450°C products is more distinct than that in 350°C ones (Figure 8a and 8b), which indicates the importance effect of temperature on behavior of Ti^{4+} in hydrothermal systems. Along the fluid flow direction, the TiO_2 rise decreased, implying that the Ti^{4+} behavior may be controlled by both temperature and ionic concentration. However, the TiO_2 increase in the 450°C products is much higher than that in the 350°C ones, which implies that temperature may be a more important controlling factor. Lead content in the 450°C products increases but remains constant in the 350°C ones, while both initial experiment fluids have the same Pb^{2+} concentration, which indicates that Pb^{2+} enter more readily into mineral lattice under high temperature. Due to the similar ionic radius, Pb^{2+} can substitute Ba^{2+} and K^+ in the mineral lattice (Liu, 1984), e.g., substituting K^+ in K-feldspar. The higher Pb content in the 450°C products may be caused by the more Pb^{2+} substitute K^+ under higher temperature, but the non-monotonic variation trends along fluid flow remains unclear and needs more studies. Strontium content increases in the 450°C products and slight decreases in the 350°C ones. Considering the substitution of Sr^{2+} for K^+ or Ca^{2+} in feldspar, we consider that this exchange reaction only occurred at above 350°C, and Sr is mainly leached at below 350°C.

4.3.2 Ore formation and potential of peripheral mineralization

Copper and S contents increase significantly in experimental products implying sulfide precipitation during the experiment. The dominant sulfide is covellite (Figure 16a), as re-

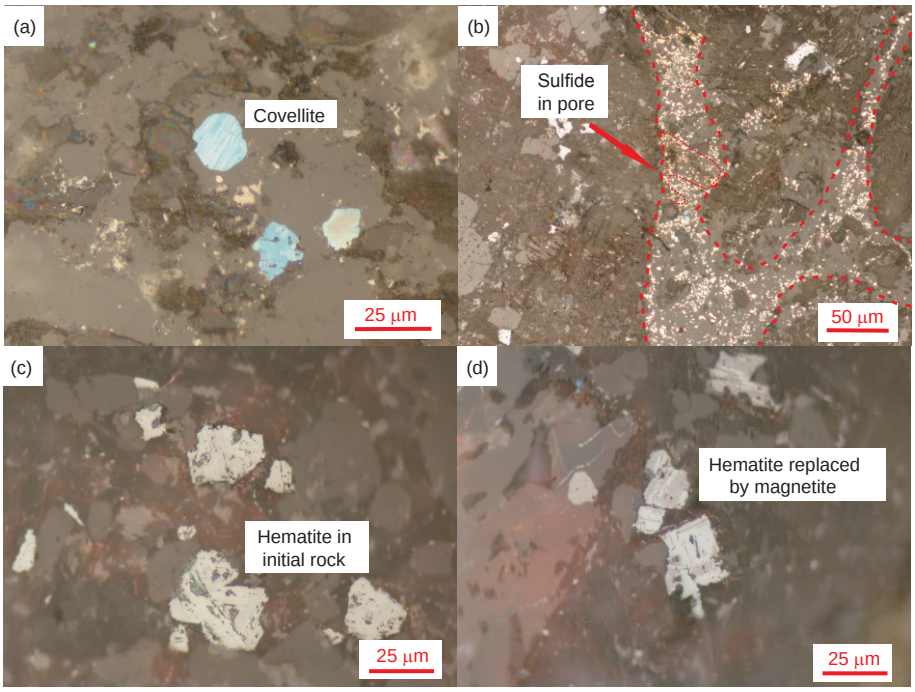

Figure 16 (Color online) Covellite (a) and fine sulfide crystals (b) in the experimental products; (c) hematite in initial rock; (d) hematite replaced by magnetite in experimental products.

vealed by microscopic observation and EPMA analysis. Some sulfides are also speculated to be pyrite or chalcopyrite (Figure 16b), but are too fine-grained to be analyzed with EPMA. The formation of sulfide in experiment products was ascribed to the relatively low oxygen fugacity provided by the nickel alloy reaction cell (composed mainly of Ni and minor Cr, Co and Fe) and the corresponding buffer reaction is $2Ni+O_2=2NiO$. Although the oxygen fugacity value cannot be quantified in the experimental system, the oxygen fugacity range of the experimental system can be roughly inferred by the mineral assemblages of the experimental products. The original hematite is partially transformed to magnetite in the products (Figure 16c and 16d), and the oxygen fugacity of experimental system cannot be below NNO. Therefore, we infer that the oxygen fugacity of the system is between NNO and HM. The oxygen fugacity decrease contributed to the reduction of SO_4^{2-} into S^{2-}, which then combined with Cu^{2+} to form covellite. The EPMA results show that Fe is leached from the mafic mineral rim in the experimental products. The leached Fe^{2+} may have reacted with Cu^{2+} and S^{2-} in the fluids to form the fine-grained chalcopyrite or pyrite. The anhydrite-sulfide assemblage occurs in the potassic alteration zone of porphyry deposits, which reflects that a relatively oxidized environment can also cause sulfide precipitation (Yang et al., 2009; Chang et al., 2018), but we consider that an oxygen fugacity decrease in the ore-forming fluids is conductive to the massive precipitation of sulfides from the pre-mineralization to the main mineralization stage. The nickel alloy reaction cell used in this experiment provided such environment, but the reason why large amount of covellite, instead of chalcopyrite and pyrite, was formed needs further studies.

The Cu and S contents in the initial fluid of the 450°C experiment is twice of that in the 350°C one, but the amount of Cu and S precipitated in the 450°C products increases by nearly 10 and 20 times, respectively, than that in the 350°C ones. This is likely associated with more intense reactions under higher temperature, during which more sulfides and anhydrites are formed. Along the fluid flow direction, the content of Cu and S in the products decrease rapidly and the extent of variation is greater under higher temperature, which may be caused by the gradual decrease of Cu and S concentrations in the fluids resulted from sulfide precipitation.

Zinc and Mn were both leached in the experimental products, especially under 450°C, and thus the Zn-Mn mobilization and transformation may be mainly controlled by temperature. As an active element, Zn can be leached from the wall rocks when the fluid contains alkali metals and halogens (Liu, 1984). Along the fluid flow direction, the degree of Zn leaching gradually increases, implying that the leaching is also affected by other factors. In porphyry Cu systems, the hydrothermal fluids leach Zn from the wall rocks (may account for a small part of the total Zn content), which may contribute to the distal Zn mineralization. The experimental results show that high-temperature fluids are more capable to transport Zn^{2+}, therefore the Zn mineralization only occurs when the transport capacity of the fluid is significantly reduced. For example, when the Zn^{2+}-rich

fluids migrate to the periphery of porphyry systems and encounter carbonate formation, the fluids cool and the metal complexes destabilize, precipitating Zn sulfides to form the Pb-Zn orebodies (Sillitoe, 1973; Heinrich, 2006).

4.4 Migration trends of elements and exploration implications

Spatial distribution features of certain trace elements in porphyry Cu systems can provide important clues to identify concealed orebodies (Cooke et al., 2017). The ore fluid temperatures gradually decrease with the outward migration, and the fluid composition is changed by continuous fluid-rock interactions. Therefore, the composition changes in the surrounding rocks record the flowing processes and pathway of the ore-forming fluids, and the hydrothermal center can be located accordingly. Correspondingly, the elemental spatial distribution and relative position in the porphyry system can be inferred based on the variation trends of these elements along the fluid flow in the experimental products. We used basaltic-andesite rocks, the most common wall rocks in porphyry systems, as rock samples in this experiment. Therefore, these indicators can be applied to the porphyry Cu systems developed in intermediate-mafic volcanic rocks.

The K_2O and TiO_2 contents in the 450°C products are significantly higher than those in the 350°C ones, and both oxides show a decreasing trend away from the hydrothermal center, which indicates that K^+ and Ti^{4+} in the fluid are more prone to enter the solid phase at higher temperature. Along the fluid flow direction, the fluid cools and K^+ and Ti^{4+} contents gradually decrease, which reduces the K_2O and TiO_2 enrichments in the wall rocks. K_2O and TiO_2 contents in the distal wall rocks are weakly affected by hydrothermal fluid and remain constant. Therefore, it can be concluded that the K_2O and TiO_2 contents in the wall rocks are high close to the high-temperature alteration zone, and decrease outward from the hydrothermal center. In the distal area of the hydrothermal system, the K_2O and TiO_2 contents are close to the background value. Na_2O is leached at upstream and enriched at downstream in the 450°C products, but the Na_2O content increase in the 350°C ones. The Na_2O variation trend in products indicates that Na_2O is mainly leached at high temperature alteration zone near hydrothermal center and is weakly enriched away from high temperature center. SiO_2 is also leached at upstream and enriched at downstream in the experimental products, and the enrichment is more sig-

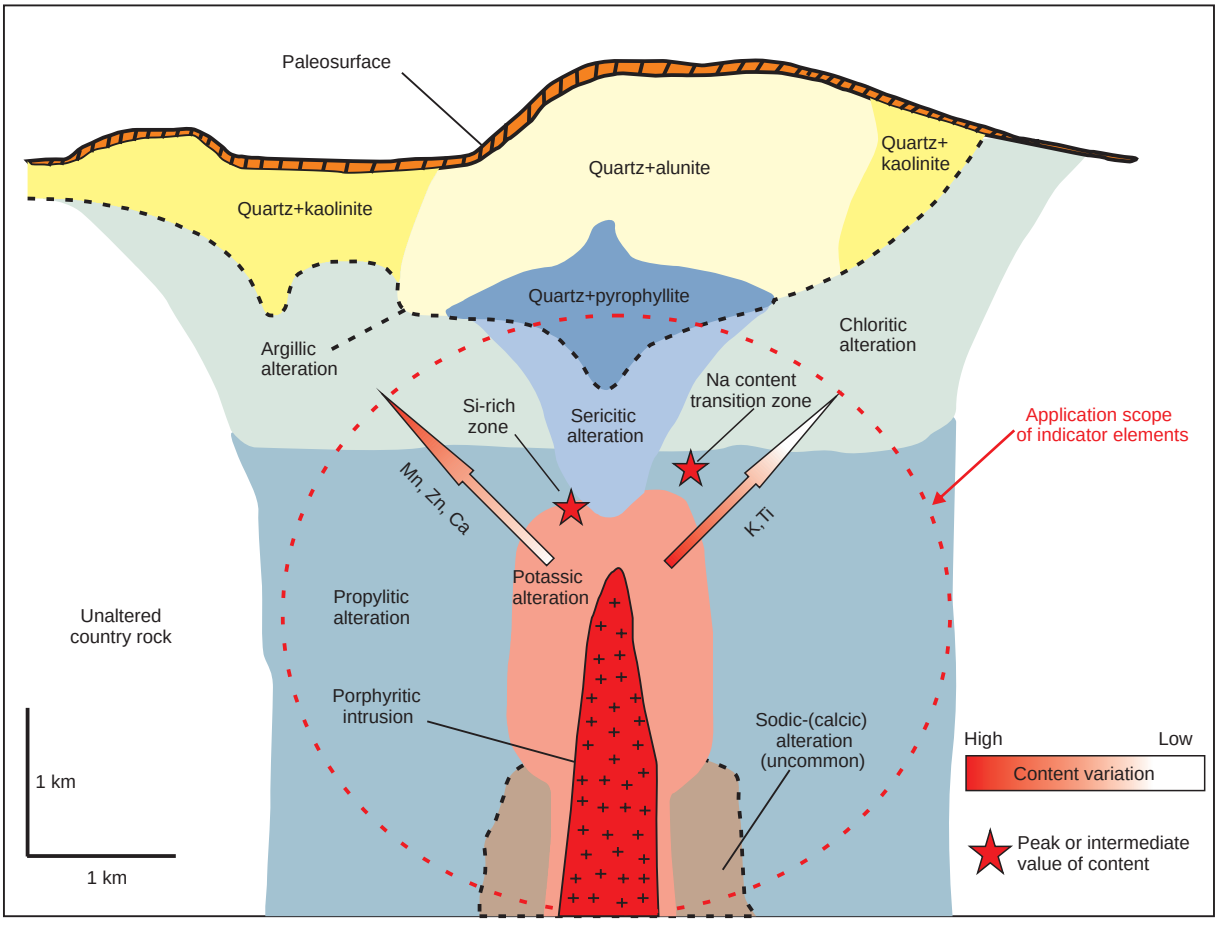

Figure 17 (Color online) Indicator element variation trends in volcanic wall rocks of porphyry Cu system. Modified after Sillitoe (2010).

nificant in the 350°C products. This trend implies that high-temperature fluids can cause significant SiO_2 loss in the wall rocks, and the cooling of the fluids during their outward migration would result in SiO_2 precipitation at the periphery of the hydrothermal system, as featured by the development of extensive quartz-rich hydrothermal veins. Calcium, Zn and Mn are all leached in the experimental products (esp. under higher temperatures), which implies that temperature is a key factor for the leaching of these elements, and that their concentrations in the wall rocks increase away from the hydrothermal center.

In summary, with increasing distance from the hydrothermal center, the K and Ti contents in the volcanic wall rocks decrease and the Ca, Mn and Zn contents have an opposite variation trend, while the Na and Si contents may reach a peak at region near high-temperature alteration zone (Figure 17). This conclusion is based on that single-sourced ore-forming fluids only react with intermediate-mafic volcanic rocks. However, the alteration zones may be superimposed and modified by other sources of fluids in the late ore formation stage, and the original elemental distribution patterns in the wall rocks may be changed. Therefore, the application of these indicators to determine the mineralization center should be carefully assessed in porphyry Cu exploration.

5. Conclusion

(1) Experimental results indicate that potassic alteration dominates over sodic alteration under higher temperature. With temperature decreasing, the potassic alteration intensity decreases but the sodic alteration intensity increases. The inhibition effect of K^+ ions on Na^+ behavior under high temperatures may led to the widespread development of potassic zone and absence of sodic zone in the core of the porphyry Cu systems.

(2) High-temperature hydrothermal alteration causes the Ca leaching of wall rocks, increasing fluid Ca and hydrothermal anhydrite content. That is also conductive to the enrichment of Mg, Zn and Mn in fluid and contributes to propylitic zone formation at distal. Heating is also important for incorporation of Ti, Sr and Pb into minerals through substitution reactions.

(3) The reaction of ore-forming fluids with the volcanic wall rocks would leach and transport majors elements from wall rocks, among which univalent and divalent cations are more readily leached than Al and Si. Exploration indicators derived from this experiment include decreasing K-Ti contents and increasing Ca-Mg-Zn contents outward from the porphyry hydrothermal center. A zone of maximum Na and Si contents may exist close to the high-temperature alteration zone.

Acknowledgements *Zhang Dongwei, Li Dengfeng, Zhang Shitao, Zhao Liandang, Xu Chao and Huang Jianhan are thanked for the laboratory assistance. We also appreciate the constructive comments from three anonymous reviewers which significantly improved this manuscript. This work was supported by National Natural Science Foundation of China (Grant No. U1603244), Strategic Priority Research Program (B) of Chinese Academy of Sciences (Grant No. XDB1803206) and Science and Technology Planning Project of Guangdong Province (Grant No. 2017B030314175).*

References

Aagaard P, Helgeson H C. 1982. Thermodynamic and kinetic constraints on reaction rates among minerals and aqueous solutions: I, Theoretical considerations. Am J Sci, 282: 237–285

Ague J J, Brimhall G H. 1989. Geochemical modeling of steady state fluid flow and chemical reaction during supergene enrichment of porphyry copper deposits. Econ Geol, 84: 506–528

Airy G B. 1855. On the computation of the effect of the attraction of mountain-masses, as disturbing the apparent astronomical latitude of stations in geodetic surveys. Philos Trans R Soc Lond, 145: 101–104

Barnes H L. 1997. Geochemistry of Hydrothermal Ore Deposits. 3rd ed. John Wiley & Sons. 1

Bondar R J, Sanchez P L, Moncada D, Macinnis M S. 2014. Fluid inclusions in hydrothermal ore deposits. Treat Geochem, 13: 119–142

Bickle M, Baker J. 1990. Migration of reaction and isotopic fronts in infiltration zones: Assessments of fluid flux in metamorphic terrains. Earth Planet Sci Lett, 98: 1–13

Bird D K, Schiffman P, Elders W A, Williams A E, McDowell S D. 1984. Calc-silicate mineralization in active geothermal systems. Econ Geol, 79: 671–695

Brimhall G H. 1977. Early fracture-controlled disseminated mineralization at Butte, Montana. Econ Geol, 72: 37–59

Carmichael D M. 1987. Induced stress and secondary mass transfer: Thermodynamic basis for the tendency toward constant-volume constraint in diffusion metasomatism. In: Helgeson H C, ed. Chemical Transport in Metasomatic Processes. NATO ASI Series (Series C: Mathematical and Physical Sciences). Dordrecht: Springer

Carten R B. 1986. Sodium-calcium metasomatism; chemical, temporal, and spatial relationships at the Yerington, Nevada, porphyry copper deposit. Econ Geol, 81: 1495–1519

Chang J, Li J W, Audétat A. 2018. Formation and evolution of multistage magmatic-hydrothermal fluids at the Yulong porphyry Cu-Mo deposit, eastern Tibet: Insights from LA-ICP-MS analysis of fluid inclusions. Geochim Cosmochim Acta, 232: 181–205

Chen H Y, Xiao B. 2014. Metallogenesis of subduction zone: The progress and future. Geosci Front, 21: 13–22

Cooke D R, Hollings P, Walshe J L. 2005. Giant porphyry deposits: Characteristics, distribution, and tectonic controls. Econ Geol, 100: 801–818

Cooke D R, Baker M, Hollings P, Sweet G, Chang Z, Danyushevsky L, Gilbert G, Zhou T, White N C, Gemmell J B, Inglis S. 2014a. New advances in detecting systems-epidote mineral chemistry as a tool for vectoring and fertility assessments. Soc Econ Geologists Spec Publ, 18: 127–152

Cooke D R, Agnew P, Hollings P. 2017. Porphyry indicator minerals (PIMS) and porphyry vectoring and fertility tools (PVFTS)-indicators of mineralization styles and recorders of hypogene geochemical dispersion halos. In: Exploration 17: Sixth Decennial International Conference on Mineral Exploration. Toronto

Cooke D R, Hollings P, Wilkinson J J, Tosdal R M. 2014b. Geochemistry of porphyry deposits. Treat Geochem, 13: 357–381

Dang Z, Hou Y. 1995. Experimental study on the dissolution kinetics of basalt-water interaction. Acta Petrol Sin, 11: 9–15

Du L T. 1986. Geochemistry of alkaline metasomatism. Sci China, 1: 83–92

Du J G. 2010. High Pressure Geoscience. Beijing: Seismological Press

Ferry J M, Dipple G M. 1991. Fluid flow, mineral reactions, and metaso-

matism. Geology, 19: 211–214
Ferry J M, Dipple G M. 1992. Models for coupled fluid flow, mineral reaction, and isotopic alteration during contact metamorphism: The Notch Peak aureole, Utah. Ame Miner, 77: 577–591
Fournier R O. 1999. Hydrothermal processes related to movement of fluid from plastic into brittle rock in the magmatic-epithermal environment. Econ Geol, 94: 1193–1211
Fournier R O, Marshall W L. 1983. Calculation of amorphous silica solubilities at 25 to 300°C and apparent cation hydration numbers in aqueous salt solutions using the concept of effective density of water. Geochim Cosmochim Acta, 47: 587–596
Frank M R, Candela P A, Piccoli P M. 1998. K-feldspar-muscovite-andalusite-quartz-brine phase equilibria: An experimental study at 25 to 60 MPa and 400 to 550°C. Geochim Cosmochim Acta, 62: 3717–3727
Frank M R, Vaccaro D M. 2012. An experimental study of high temperature potassic alteration. Geochim Cosmochim Acta, 83: 195–204
Gautier J M, Oelkers E H, Schott J. 1994. Experimental study of K-feldspar dissolution rates as a function of chemical affinity at 150°C and pH 9. Geochim Cosmochim Acta, 58: 4549–4560
Gislason S R, Oelkers E H. 2003. Mechanism, rates, and consequences of basaltic glass dissolution: II. An experimental study of the dissolution rates of basaltic glass as a function of pH and temperature. Geochim Cosmochim Acta, 67: 3817–3832
Gudbrandsson S, Wolff-Boenisch D, Gislason S R, Oelkers E H. 2011. An experimental study of crystalline basalt dissolution from 2≤pH≤11 and temperatures from 5 to 75°C. Geochim Cosmochim Acta, 75: 5496–5509
Harris N B W, Inger S, Ronghua X. 1990. Cretaceous plutonism in Central Tibet: An example of post-collision magmatism? J Volcanol Geotherm Res, 44: 21–32
Halter W E, Pettke T, Heinrich C A. 2002. The origin of Cu/Au ratios in porphyry-type ore deposits. Science, 296: 1844–1846
Haselton Jr H T, Cygan G L, Jenkins D M. 1995. Experimental study of muscovite stability in pure H_2O and 1 molal KCl-HCl solutions. Geochim Cosmochim Acta, 59: 429–442
Helgeson H C. 1969. Thermodynamics of hydrothermal systems at elevated temperatures and pressures. Am J Sci, 267: 729–804
Heinrich C A. 1990. The chemistry of hydrothermal tin(-tungsten) ore deposition. Econ Geol, 85: 457–481
Heinrich C A. 2005. The physical and chemical evolution of low-salinity magmatic fluids at the porphyry to epithermal transition: A thermodynamic study. Miner Deposita, 39: 864–889
Heinrich C A. 2006. From fluid inclusion microanalysis to large-scale hydrothermal mass transfer in the Earth's interior. J Mineral Petrol Sci, 101: 110–117
Hemley J J, Montoya J W, Marinenko J W, Luce R W. 1980. Equilibria in the system Al_2O_3-SiO_2-H_2O and some general implications for alteration/mineralization processes. Econ Geol, 75: 210–228
Heinrich C A, Walshe J L, Harrold B P. 1996. Chemical mass transfer modelling of ore-forming hydrothermal systems: Current practise and problems. Ore Geol Rev, 10: 319–338
Hemley J J. 1959. Some mineralogical equilibria in the system K_2O-Al_2O_3-SiO_2-H_2O. Am J Sci, 257: 241–270
Hemley J J, Jones W R. 1964. Chemical aspects of hydrothermal alteration with emphasis on hydrogen metasomatism. Econ Geol, 59: 538–569
Hildreth W, Moorbath S. 1988. Crustal contributions to arc magmatism in the Andes of central Chile. Contr Mineral Petrol, 98: 455–489
Holyland P W. 1987. Dynamic modelling at the Renison tin mine. Pacific Rim Congress'87. 189–193
Hu S M, Zhang R H, Zhang X T, Hang W B. 2010. Experimental study of water-basalt interaction in Luzong volcanic basin and its application. Acta Petrol Sin, 26: 2681–2693
Huang W B, Zhang R H, Hu S M. 2011. Chemical dynamics of basalt-seawater interaction near critical states. Acta Mineral Sin, Suppl: 692
Hutcheon I, Shevalier M, Abercrombie H J. 1993. pH buffering by metastable mineral-fluid equilibria and evolution of carbon dioxide fugacity during burial diagenesis. Geochim Cosmochim Acta, 57: 1017–1027
Kerrich R. 2000. The geodynamics of world-class gold deposits, characteristics, space-time distribution, and origins. Rev. Econ Geol, 13: 501–551
Korzhinskii D S. 1959. Acid-basic interaction of components in silicate melts and the direction of the cotectic lines. Doklady Akademii Nauk SSSR, 128: 383–386
Korzhiniskii D S. 1970. Theory of Metasomatie Zoning. Oxford: Oxford University Press
Landtwing M R, Pettke T, Halter W E, Heinrich C A, Redmond P B, Einaudi M T, Kunze K. 2005. Copper deposition during quartz dissolution by cooling magmatic-hydrothermal fluids: The Bingham porphyry. Earth Planet Sci Lett, 235: 229–243
Landtwing M R, Furrer C, Redmond P B, Pettke T, Guillong M, Heinrich C A. 2010. The Bingham Canyon porphyry Cu-Mo-Au deposit. III. Zoned copper-gold ore deposition by magmatic vapor expansion. Econ Geol, 105: 91–118
Liang H Y, Sun W, Su W C, Zartman R E. 2009. Porphyry copper-gold mineralization at Yulong, China, promoted by decreasing redox potential during magnetite alteration. Econ Geol, 104: 587–596
Lasaga A C, Rye D M. 1993. Fluid flow and chemical reaction kinetics in metamorphic systems. Am J Sci, 293: 361–404
Liu Y, Liu H C, Li X H. 1996. Simultaneous and precise determination of 40 trace elements in rock Samples using ICP-MS. Geochimica, 6: 552–558
Liu Y J. 1984. Geochemistry of Elements. Beijing: Science Press
Liu Y S, Zhang G L. 1996. An Experimental study on sea water-basalt interaction at 250–500°C and 100 MPa. Geochimica, 1: 53–62
Lowell J D, Guilbert J M. 1970. Lateral and vertical alteration-mineralization zoning in porphyry ore deposits. Econ Geol, 65: 373–408
Luhmann A J, Tutolo B M, Tan C, Moskowitz B M, Saar M O, Seyfried Jr. W E. 2017. Whole rock basalt alteration from CO_2-rich brine during flow-through experiments at 150°C and 150 bar. Chem Geol, 453: 92–110
Merino E, Moore C, Ortoleva P, Ripley E. 1986. Mineral zoning in sediment-hosted copper-iron sulfide deposits—A quantitative kinetic approach. In: Geology and Metallogeny of Copper Deposits. Special Publication No. 4 of the Society for Geology Applied to Mineral Deposits. Berlin: Springer. 559–571
Montoya J W, Hemley J J. 1975. Activity relations and stabilities in alkali feldspar and mica alteration reactions. Econ Geol, 70: 577–583
Mottl M J, Holland H D. 1978. Chemical exchange during hydrothermal alteration of basalt by seawater—I. Experimental results for major and minor components of seawater. Geochim Cosmochim Acta, 42: 1103–1115
Murphy W M, Oelkers E H, Lichtner P C. 1989. Surface reaction versus diffusion control of mineral dissolution and growth rates in geochemical processes. Chem Geol, 78: 357–380
Nash J T. 1976. Fluid-inclusion petrology—Data from porphyry copper deposits and applications to exploration: A summary of new and published descriptions of fluid inclusions from 36 porphyry copper deposits and discussion of possible applications to exploration for copper deposits. US Govt. Print. Off
Oelkers E H. 2001. General kinetic description of multioxide silicate mineral and glass dissolution. Geochim Cosmochim Acta, 65: 3703–3719
Oelkers E H, Schott J. 2001. An experimental study of enstatite dissolution rates as a function of pH, temperature, and aqueous Mg and Si concentration, and the mechanism of pyroxene/pyroxenoid dissolution. Geochim Cosmochim Acta, 65: 1219–1231
Oelkers E H, Schott J, Devidal J L. 1994. The effect of aluminum, pH, and chemical affinity on the rates of aluminosilicate dissolution reactions. Geochim Cosmochim Acta, 58: 2011–2024
Orville P M. 1962. Alkali metasomatism and feldspars. Norsk Geologisk Tidsskrift. 283–316
Pollard P J. 2001. Sodic(-calcic) alteration in Fe-oxide-Cu-Au districts: An origin via unmixing of magmatic H_2O-CO_2-NaCl±$CaCl_2$-KCl fluids. Miner Depos, 36: 93–100

Ré C L, Kaszuba J P, Moore J N, McPherson B J. 2014. Fluid-rock interactions in CO_2-saturated, granite-hosted geothermal systems: Implications for natural and engineered systems from geochemical experiments and models. Geochim Cosmochim Acta, 141: 160–178
Reed M H. 1997. Hydrothermal alteration and its relationship to ore fluid composition. Geochem Hydrothermal Ore Deposits, 1: 303–365
Redmond P B, Einaudi M T, Inan E E, Landtwing M R, Heinrich C A. 2004. Copper deposition by fluid cooling in intrusion-centered systems: New insights from the Bingham porphyry ore deposit, Utah. Geology, 32: 217–220
Redmond P B, Einaudi M T. 2010. The Bingham Canyon porphyry Cu-Mo-Au deposit. I. Sequence of intrusions, vein formation, and sulfide deposition. Econ Geol, 105: 43–68
Richards J P. 2011. Magmatic to hydrothermal metal fluxes in convergent and collided margins. Ore Geol Rev, 40: 1–26
Richards J P, Kerrich R. 2007. Special paper: Adakite-like rocks: Their diverse origins and questionable role in metallogenesis. Econ Geol, 102: 537–576
Ringwood A E. 1977. Petrogenesis in Island Arc Systems. Island Arcs, Deep Sea Trenches and Back-arc Basins. Washington: American Geophysical Union. 311–324
Roedder E. 1971. Fluid inclusion studies on the porphyry-type ore deposits at Bingham, Utah, Butte, Montana, and Climax, Colorado. Econ Geol, 66: 98–118
Rogers K L, Neuhoff P S, Pedersen A K, Bird D K. 2006. CO_2 metasomatism in a basalt-hosted petroleum reservoir, Nuussuaq, West Greenland. Lithos, 92: 55–82
Rusk B G, Reed M H, Dilles J H, Klemm L M, Heinrich C A. 2004. Compositions of magmatic hydrothermal fluids determined by LA-ICP-MS of fluid inclusions from the porphyry copper-molybdenum deposit at Butte, MT. Chem Geol, 210: 173–199
Rusk B G, Reed M H, Dilles J H. 2008. Fluid inclusion evidence for magmatic-hydrothermal fluid evolution in the porphyry copper-molybdenum deposit at Butte, Montana. Econ Geol, 103: 307–334
Schott J, Pokrovsky O S, Oelkers E H. 2009. The link between mineral dissolution/precipitation kinetics and solution chemistry. Rev Mineral Geochem, 70: 207–258
Seedorff E, Dilles J H, Proffett J M. 2005. Porphyry deposits: Characteristics and origin of hypogene features. Econ Geol, 100: 251–298
Sillitoe R H. 1972. A plate tectonic model for the origin of porphyry copper deposits. Econ Geol, 67: 184–197
Sillitoe R H. 1973. The tops and bottoms of porphyry copper deposits. Econ Geol, 68: 799–815
Sillitoe R H. 2010. Porphyry copper systems. Econ Geol, 105: 3–41
Stern C R, Funk J A, Skewes M A, Arevalo A. 2007. Magmatic anhydrite in plutonic rocks at the El Teniente Cu-Mo deposit chile, and the role of sulfur- and copperrich magmas in its formation. Econ Geol, 102: 1335–1344
Sun S, McDonough W F. 1989. Chemical and isotopic systematics of oceanic basalts: Implications for mantle composition and processes. Geol Soc Lond Spec Publ, 42: 313–345
Sun W D, Ling M X, Yang X Y, Fan W M, Ding X, Liang H Y. 2010. Ridge subduction and porphyry copper-gold mineralization: An overview. Sci China Earth Sci, 53: 475–484
Sverjensky D A, Hemley J J, D'angelo W M. 1991. Thermodynamic assessment of hydrothermal alkali feldspar-mica-aluminosilicate equilibria. Geochim Cosmochim Acta, 55: 989–1004
Tan K X, Zhang Z R, Wang Z G. 1994. The Mechanism of surface chemical kinetics of dissolution of minerals. Acta Mineral Sin, 3: 207–214
Wang Y F, Chen H Y, Xiao B, Han J S. 2016. Porphyritic-overlapped mineralization of Tuwu and Yandong copper deposits in Eastern Tianshan Mountains, Xinjiang. Mineral Deposits, 35: 51–68
Wang Y R, Wang Z X, Zhang S. 2000. Water-rock reaction experiment and mineralization. Bull Mineral Petrol Geochem, 19: 426–427
Wilkinson J J, Chang Z, Cooke D R, Baker M J, Wilkinson C C, Inglis S, Chen H, Bruce Gemmell J. 2015. The chlorite proximitor: A new tool for detecting porphyry ore deposits. J Geochem Exploration, 152: 10–26
Winkler H G F, von Platen H. 1961. Experimentelle gesteinsmetamorphose —V. Geochim Cosmochim Acta, 24: 250–259
Xiao B, Chen H Y, Hollings P, Han J S, Wang Y F, Yang J T, Cai K D. 2015. Magmatic evolution of the Tuwu-Yandong porphyry Cu belt, NW China: Constraints from geochronology, geochemistry and Sr-Nd-Hf isotopes. Gondwana Res, 43: 74–91
Yang Z, Hou Z, White N C, Chang Z S, Li Z Q, Song Y C. 2009. Geology of the post-collisional porphyry copper-molybdenum deposit at Qulong, Tibet. Ore Geol Rev, 36: 133–159
Zhang D H, Xu J H, Yu X Q, Li J K, Mao S D, Wang K Q, Li Y Q. 2011. The diagenetic and metallogenic depth: Main constraints and the estimation methods. Geol Bull China, 30: 112–125
Zhang Y X. 2010. Geochemical Kinetics. Beijing: Higher Education Press

(Responsible editor: Huaiwei NI)